Mathematical modelling of cell layer growth in a hollow fibre bioreactor☆

Lloyd A.C. Chapman[a,b,∗], Jonathan P. Whiteley[b], Helen M. Byrne[a,b], Sarah L. Waters[a], Rebecca J. Shipley[c]

[a] Mathematical Institute, University of Oxford, Andrew Wiles Building, Radcliffe Observatory Quarter, Woodstock Road, Oxford OX2 6GG, UK
[b] Department of Computer Science, University of Oxford, Wolfson Building, Parks Road, Oxford OX1 3QD, UK
[c] Department of Mechanical Engineering, University College London, Torrington Place, London WC1E 7JE, UK

ABSTRACT

Generating autologous tissue grafts of a clinically useful volume requires efficient and controlled expansion of cell populations harvested from patients. Hollow fibre bioreactors show promise as cell expansion devices, owing to their potential for scale-up. However, further research is required to establish how to specify appropriate hollow fibre bioreactor operating conditions for expanding different cell types. In this study we develop a simple model for the growth of a cell layer seeded on the outer surface of a single fibre in a perfused hollow fibre bioreactor. Nutrient-rich culture medium is pumped through the fibre lumen and leaves the bioreactor via the lumen outlet or passes through the porous fibre walls and cell layer, and out via ports on the outer wall of the extra-capillary space. Stokes and Darcy equations for fluid flow in the fibre lumen, fibre wall, cell layer and extra-capillary space are coupled to reaction–advection–diffusion equations for oxygen and lactate transport through the bioreactor, and to a simple growth law for the evolution of the free boundary of the cell layer. Cells at the free boundary are assumed to proliferate at a rate that increases with the local oxygen concentration, and to die and detach from the layer if the local fluid shear stress or lactate concentration exceed critical thresholds. We use the model to predict operating conditions that maximise the cell layer growth for different cell types. In particular, we predict the optimal flow rate of culture medium into the fibre lumen and fluid pressure imposed at the lumen outlet for cell types with different oxygen demands and fluid shear stress tolerances, and compare the growth of the cell layer when the exit ports on the outside of the bioreactor are open with that when they are closed. Model simulations reveal that increasing the inlet flow rate and outlet fluid pressure increases oxygen delivery to the cell layer and, therefore, the growth rate of cells that are tolerant to high shear stresses, but may be detrimental for shear-sensitive cells. The cell layer growth rate is predicted to increase, and be less sensitive to the lactate tolerance of the cells, when the exit ports are opened, as the radial flow through the bioreactor is enhanced and the lactate produced by the cells cleared more rapidly from the cell layer.

1. Introduction

The aim of *in vitro* tissue engineering is to produce cells and tissues in the laboratory that can be used to replace or repair damaged or lost tissues in a patient's body. Generating these cells and tissues from the patient's own cells (autologous cells) has several advantages, including decreased likelihood of immune rejection, but requires expansion of the original cell population taken from the patient. This can be achieved by seeding the cells onto a biomaterial scaffold and incubating the cell-scaffold construct in a bioreactor.

Hollow fibre bioreactors (HFBs) show great promise as cell expan-

sion devices. They consist of a cylindrical glass module housing a single or multiple porous, hollow, biodegradable polymer fibres. Nutrient-rich culture medium is pumped through the fibre lumen(s) and forced through the fibre wall(s) (membranes) to cells seeded in the surrounding space (the extra-capillary space or ECS). There are ports at either end of the ECS, which may be opened to promote radial flow through the bioreactor, or left closed (see Fig. 1). With the ECS ports open, and hence at atmospheric pressure, the flow through the membrane is controlled by fixing the fluid pressure at the downstream lumen outlet, and this allows the nutrient delivery and fluid shear stress experienced by the cells in the ECS to be controlled. Cells can either be seeded
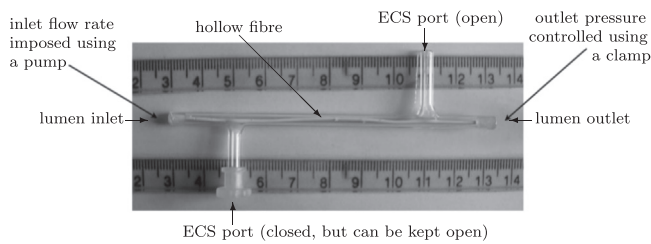
Fig. 1. Photograph of a single-fibre HFB module. ECS=extra-capillary space. Adapted from Shipley and Waters (2012).

directly onto the outer surface of the fibres, or in a hydrogel throughout the ECS (Wung et al., 2014). As well as enabling the chemical and mechanical environment of the cells to be controlled, HFBs provide a highly efficient means of expanding cells due to the large surface area of the fibres available for cell proliferation relative to the bioreactor volume—as many cells can be cultured in a 0.5 l HFB as in a 1000 l standard culture flask (Wung et al., 2014).

Despite these advantages, there is still potential to improve operation and scale up of HFBs for clinical use. In particular, better understanding of the combined effects of cell seeding and operating conditions on cell population growth in HFBs is required. Mathematical modelling of cell growth in HFBs can help significantly in this regard by predicting parameter ranges for which growth is maximised, and thereby streamlining the choice of parameters and operating conditions to test experimentally, saving time and money. In this study we focus on the relatively simple single-fibre HFB shown in Fig. 1, to gain deeper insight into the factors that affect growth.

Experiments with the single-fibre HFB have shown that cells seeded onto the outer surface of the fibre will proliferate over the surface until they reach confluence given the right culture conditions and culture period (Ellis and Chaudhuri, 2007; Meneghello, 2010). Additionally, once cells have reached confluence, they can proliferate outwards into the ECS to establish a tissue layer multiple cells deep (Tharakan and Chau, 1986; Lu et al., 2005; Ye et al., 2007; De Napoli et al., 2011). Although oxygen concentration, lactate concentration and fluid shear stress are known to affect the rate of cell proliferation and death, how they interact and affect the rate and extent of cell layer growth into the ECS have not yet been investigated. This is the primary purpose of our study, which will be achieved through mathematical modelling.

Previous modelling studies of HFBs have focussed on describing fluid and solute transport through the bioreactor (Kelsey et al., 1990; Piret and Cooney, 1991; Sullivan et al., 2006; Shipley et al., 2010, 2011; Ye et al., 2006) and considered the timescales associated with these transport processes rather than the longer timescale associated with cell proliferation (see Shipley et al., 2010, 2011; Brotherton and Chau, 1996 for more detailed reviews). Hence the effects of cell proliferation on fluid flow and solute transport in the bioreactor have generally been ignored. Most transport models for HFBs are based on the Krogh cylinder approximation (Brotherton and Chau, 1996). In Krogh cylinder models, the flow and mass transport in the fibre lumen are modelled using the Stokes flow equations and advection–diffusion equations respectively, and convection effects in the membrane and ECS are usually ignored, which is representative of the HFB set-up in Fig. 2(a) with the ECS ports closed. When flow through the membrane and ECS has been considered (which is relevant when one or more ECS ports are open), it has been modelled using Darcy's law, and nutrient uptake and waste product synthesis have been described by adding appropriate reaction terms to the ECS mass transport equations. In terms of nutrient transport and consumption, oxygen is the most widely modelled solute (Schonberg and Belfort, 1987; Piret and Cooney, 1991; Patzer II, 2004; Sullivan et al., 2006; Davidson et al., 2010; Shipley et al., 2011; Pearson et al., 2014), but glucose (Ye et al., 2006; Abdullah et al., 2009; Das, 2007) and proteins (Labecki et al., 1996, 2004; Shipley et al., 2009) have also been considered. By

contrast, the transport of lactate, a waste product of cell metabolism toxic to cells in high concentrations, has only been modelled recently (Shipley and Waters, 2012).

Shipley and Waters (2012) developed a model of fluid flow and oxygen and lactate transport in a single-fibre HFB with a cell-packed ECS in the absence of growth, and predicted that improving oxygen delivery to, and lactate removal from, the cells by opening the ECS ports would enable a larger cell population to be cultured in the bioreactor. Here we extend their model to allow for a non-uniform growing layer of cells attached to the outer surface of the fibre in the ECS. We assume that the rate of growth of the cell layer depends on the local oxygen and lactate concentrations and the fluid shear stress experienced by the cells. We consider both the flow configuration in which the ECS ports are closed (no flow in the membrane or ECS) and that in which they are open (flow throughout the bioreactor). The lumen outlet pressure controls the ratio of the flow through the membrane to that through the lumen. Although promoting radial flow through the bioreactor improves oxygen delivery and lactate removal to and from the cells, it also increases the shear stresses that the cells are exposed to, which can lead to cell death and detachment from the cell layer. Incorporating the effect of excess shear stress on the cell layer growth allows us to predict the optimal lumen inlet flow rate and lumen outlet pressure to maximise the growth of the cell layer for cells with different nutrient demands and sensitivity to shear stress. Modelling lactate transport and cell death due to excess lactate allows us to investigate the sensitivity of the cell layer growth to the lactate tolerance of the cells.

In addition to being the first model for a freely growing cell layer in a HFB, the work presented here differs from most previous theoretical studies of cell culture in HFBs in two key respects. First it accounts for the potentially negative effects on growth of high shear stress from high lumen inlet flow rates and lumen outlet pressures. Second it considers the feedback effect of tissue growth on fluid flow and solute transport in the bioreactor. The only other studies that have considered these effects are the multiphase models of cell culture in the single-fibre HFB of Pearson et al. (2014, 2015a,b) and our previous study on cell population expansion in the single-fibre HFB (Chapman et al., 2014). Multiphase models are continuum models that account for interactions between the flow, solute transport and cells by treating the cells and culture medium as separate phases with their own time- and space-dependent volume fractions. Mass transfer between the phases is described using constitutive source/sink terms in the mass conservation equations for each phase. Pearson et al. (2015b) used a 2D multiphase framework to describe shear-stress-dependent proliferation in a cell layer of constant depth in a HFB. They used the model to predict the effects of altering the flow rate into the ECS and the cell layer depth on the cell yield. We take a different approach here, by assuming that there is no movement of cells within the cell layer and that cell proliferation and death are localised to its outer surface, where they induce growth/recession of the cell layer, with the cell volume fraction in the cell layer remaining fixed. In our previous study (Chapman et al., 2014), we developed a 2D model of oxygen- and shear-stress-dependent cell aggregate growth along the outer surface of the fibre in a single-fibre HFB, applicable to the initial stages of cell culture, and used it to predict the lumen inlet flow rate, lumen outlet pressure and initial seeding distribution that minimised the time taken for the aggregates to reach confluence over the fibre surface. The model developed here is applicable to a later stage of cell culture, after the cells have reached confluence, when they are proliferating out into the ECS. The modelling framework presented here is similar to that used in Chapman et al. (2014), with equations for fluid and solute transport through the bioreactor coupled to equations representing cell population growth. However, here we consider an axisymmetric cylindrical geometry with a distinct cell layer rather than a simplified 2D geometry with cell aggregates, and employ additional equations to describe the fluid flow and solute transport through the cell layer as well as its
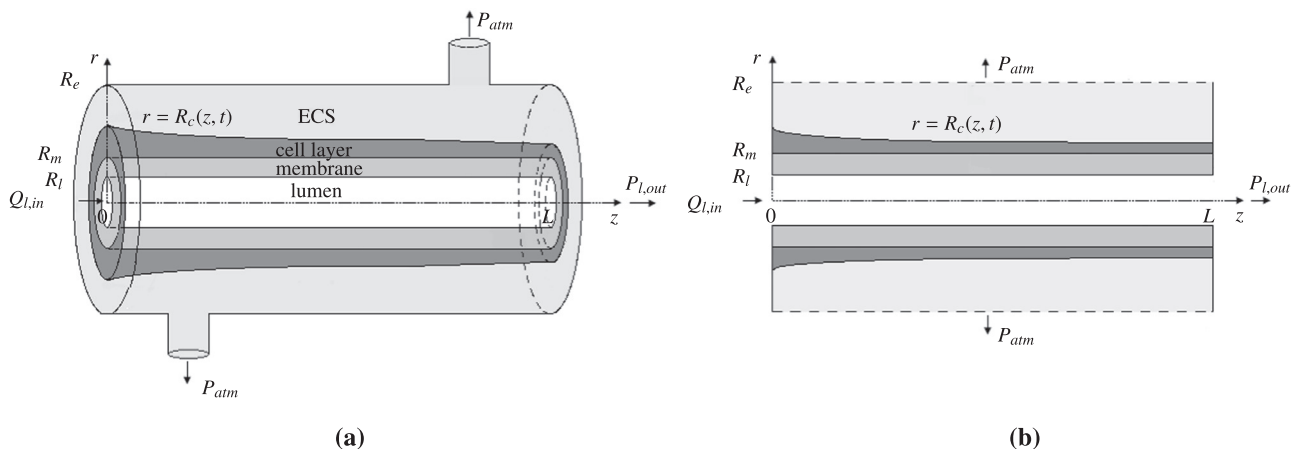
Fig. 2. (a) Schematic of the single-fibre HFB module with a cell layer on the outer surface of the fibre and open ECS ports. (b) 2D cross-section of the model set-up showing the distributed ECS port. Arrows show the direction of fluid flow into the lumen and out of the lumen outlet and ECS port(s). Notation as described in main text.

growth. In addition to using the model to predict the optimal lumen inlet flow rate and lumen outlet pressure to maximise the growth of the cell layer, we also briefly explore the potential impact of non-uniformity in the initial cell layer depth on its subsequent growth.

The paper is organised as follows. The model set-up and governing equations for the system with the ECS ports open are presented in Section 2. Model parameterisation, reduction and solution are summarised in Section 3 (further details can be found in the Appendices). In Section 4 we compare the fluid flow and oxygen and lactate distributions for static cell layers of uniform depth and non-uniform depth, and describe how the flow and solute distributions change over time for a growing cell layer. We then present the results of simulations of cell layer growth for different cell types, including predictions of the optimal lumen inlet flow rate and lumen outlet pressure for growth. We summarise the key differences in the flow, solute transport and growth when the ECS ports are closed in Section 5. In Section 6 we discuss our key findings and suggest possible model extensions.

2. Model description

2.1. Model set-up

Fig. 2(a) shows a schematic of the single-fibre HFB set-up with a cell layer surrounding the fibre. We assume that the lumen is cylindrical with a circular cross-section and that the fibre, cell layer and ECS are coaxial and annular in cross-section. For simplicity, we view the flow and solute distributions as symmetric about the lumen axis, and treat the ECS ports as being distributed over the whole of the outer wall of the ECS following Shipley et al. (2010) and Shipley and Waters (2012) (Fig. 2(b)). The system can therefore be described using axisymmetric cylindrical polar coordinates (r, z), where r is the radial distance from the lumen axis and z is the distance along the lumen axis from the inlet at $z=0$ to the outlet at $z=L$. The corresponding unit vectors in the r- and z-directions are denoted by $\mathbf{e}_r$ and $\mathbf{e}_z$. The radius of the lumen and outer radii of the fibre and ECS are denoted by R_l, R_m and R_e.

Culture medium is pumped into the lumen inlet at a prescribed volumetric flow rate $Q_{l,in}$ and a pressure $P_{l,out}$ is imposed on the fluid at the lumen outlet. When the ECS ports are open, $P_{l,out}$ controls the ratio of the flow through the membrane to that down the lumen.

Oxygen enters the system at constant concentration C_{in} via the culture medium pumped into the lumen inlet, is transported through the bioreactor by a combination of advection and diffusion, and is consumed by the cells in the cell layer. Lactate is produced by the cells in the cell layer as a by-product of respiration and transported out of the system by advection and diffusion. While high oxygen levels

promote proliferation, excess lactate causes cell death.

Cell proliferation and death are assumed to be localised to the outer surface of the cell layer, and to occur at a rate dependent on the local oxygen and lactate concentrations and interstitial fluid shear stress. As the cell layer grows or recedes, the flow, oxygen uptake and lactate production change, and this in turn affects the growth. Thus, the radial position of the outer surface of the cell layer, R_c, varies with axial position and time, i.e. $R_c = R_c(z, t)$.

Typically $L \approx 10$ cm, $R_l \approx 100$–200 μm, $(R_m - R_l) \approx 200$–400 μm and $R_e \approx 1$ mm. The aspect ratio of the fibre lumen, ϵ, is therefore very small

$$\epsilon = \frac{R_l}{L} \approx 2 \times 10^{-3} \ll 1, \tag{1}$$

as are those of the membrane, cell layer and ECS. We exploit this fact to simplify the model of the fluid flow, solute transport and cell layer growth given in Sections 2.2.1–2.2.3, so that we can make analytical progress in solving the model.

2.2. Governing equations

The model for the cell layer growth is composed of equations describing the fluid flow through the bioreactor (Section 2.2.1), equations for the transport and consumption/production of oxygen and lactate overlaid on the fluid transport model (Section 2.2.2), and equations for the growth of the cell layer coupled to the fluid and solute transport equations (Section 2.2.3). All values for the parameters that appear in the following equations, the dimensional analysis of the model, and an explanation of how parameters unobtainable from the literature were estimated are given in Section 3, and Appendices A and B.

2.2.1. Fluid transport

The flow in the lumen and ECS can be modelled as steady, incompressible Stokes flow:

$$\nabla \cdot \mathbf{u}_i = 0, \quad \mu \nabla^2 \mathbf{u}_i = \nabla p_i \quad \text{for } i = l, e, \tag{2}$$

where $\mathbf{u}_i$ ($i = l, e$) and p_i ($i = l, e$) are the fluid velocity and pressure in the lumen and ECS (denoted by subscripts l and e), and μ is the dynamic fluid viscosity.

Following several other authors (Brotherton and Chau, 1996; Ye et al., 2006; Abdullah and Das, 2007; Shipley and Waters, 2012), we model the membrane and cell layer as rigid porous media and describe the fluid flow through them using the incompressible Darcy flow equations

$$\nabla \cdot (\phi_i \mathbf{u}_i) = 0, \quad \phi_i \mathbf{u}_i = -\frac{k_i}{\mu} \nabla p_i, \quad i = m, c, \tag{3}$$

Table 1

Typical bioreactor dimensions, fluid transport parameter values and mass transport parameter values for the single-fibre HFB module.

Parameter	Description	Typical value	Reference
Bioreactor dimensions			
R_l	Lumen radius	200 μm	Shipley et al. (2010)
R_m	Fibre outer radius	400 μm	Shipley et al. (2010)
R_e	ECS outer radius	1000 μm	Shipley et al. (2010)
L	Lumen length	10 cm	Shipley et al. (2010)
Fluid transport			
ρ	Fluid density	$1000 \ \mathrm{kg \ m^{-3}}$	Elert (2015)
μ	Fluid dynamic viscosity	$1.00 \times 10^{-3} \ \mathrm{Pa \ s}$	Elert (2015)
ϕ_m	Membrane porosity	0.77	Meneghello et al. (2009)
ϕ_c	Membrane porosity	0.6	Shipley and Waters (2012)
k_m	Membrane permeability	$2.39 \times 10^{-16} \ \mathrm{m^2}$	Chapman et al. (2014)
k_c	Cell layer permeability	$7.5 \times 10^{-13} \ \mathrm{m^2}$	Appendix B.1
$Q_{l,in}$	Lumen inlet flow rate	3.33×10^{-10}–$3.33 \times 10^{-8} \ \mathrm{m^3 \ s^{-1}}$ (0.2–2 ml min^{-1})	Shipley et al. (2010), Shipley and Waters (2012)
$U = Q_{l,in}/(2\pi R_l^2)$	Typical axial lumen flow velocity	0.013–$0.13 \ \mathrm{m \ s^{-1}}$	–
$P_{l,out}$	Lumen outlet pressure	1.027×10^5–$2.068 \times 10^5 \ \mathrm{Pa}$ (14.9–30.0 psi)[*]	Shipley et al. (2010)
P_{atm}	Atmospheric pressure	$1.013 \times 10^5 \ \mathrm{Pa}$ (14.7 psi)	Elert (2015)
Mass transport			
Oxygen			
D_l	Lumen diffusivity	$3 \times 10^{-9} \ \mathrm{m^2 \ s^{-1}}$	Shipley and Waters (2012)
D_m	Membrane diffusivity	$3 \times 10^{-10} \ \mathrm{m^2 \ s^{-1}}$	Shipley and Waters (2012)
D_c	Cell layer diffusivity	$6 \times 10^{-9} \ \mathrm{m^2 \ s^{-1}}$	Shipley and Waters (2012)
D_e	ECS diffusivity	$3 \times 10^{-9} \ \mathrm{m^2 \ s^{-1}}$	Shipley and Waters (2012)
Lactate			
D_l	Lumen diffusivity	$1.4 \times 10^{-9} \ \mathrm{m^2 \ s^{-1}}$	Holm et al. (1981)
D_m	Membrane diffusivity	$1.4 \times 10^{-10} \ \mathrm{m^2 \ s^{-1}}$	[†]
D_c	Cell layer diffusivity	$6 \times 10^{-9} \ \mathrm{m^2 \ s^{-1}}$	Eggleton et al. (1928)
D_e	ECS diffusivity	$1.4 \times 10^{-9} \ \mathrm{m^2 \ s^{-1}}$	Holm et al. (1981)

[*] In all simulations $P_{l,out}$ is chosen below the threshold pressure at which there is backflow at the lumen outlet for the chosen lumen inlet flow rate.

[†] No experimental data, so $D_m = 0.1 D_l$ assumed for lactate from relationship for oxygen.

where subscripts m and c denote the membrane and cell layer, ϕ_i ($i = m, c$) are the membrane and cell layer porosities (assumed constant since the cell volume fraction in the cell layer is taken to be fixed), $\mathbf{u}_i$ and p_i ($i = m, c$) are the interstitial fluid velocities and pressures (averaged over the fluid volume), and k_i ($i = m, c$) are the fluid permeabilities of the membrane and cell layer.

We now give the boundary conditions for the fluid transport: first those on the interfaces between the lumen, membrane, cell layer and ECS and on the outer wall of the ECS, and then the axial boundary conditions at the ends of each region. For these boundary conditions, we require the definition of the fluid stress tensors in the different regions, σ_i ($i = l, m, c, e$), corresponding to Eqs. (2) and (3)

$$\sigma_i = -p_i \mathbf{I} + \mu (\nabla \mathbf{u}_i + (\nabla \mathbf{u}_i)^T), \quad i = l, e, \tag{4}$$

$$\sigma_i = -p_i \mathbf{I}, \quad i = m, c. \tag{5}$$

At the lumen–membrane and membrane–cell layer interfaces we prescribe continuity of normal fluid velocity and normal stress. Following previous studies (Shipley and Waters, 2012; Pearson et al., 2014, 2015b), we assume that the stress is transmitted via the fluid phase, so that the continuity conditions at the lumen–membrane and membrane–cell layer interfaces are

$$\mathbf{u}_l \cdot \mathbf{e}_r = \phi_m \mathbf{u}_m \cdot \mathbf{e}_r, \quad \mathbf{e}_r \cdot \sigma_l \cdot \mathbf{e}_r = \mathbf{e}_r \cdot \sigma_m \cdot \mathbf{e}_r \ \text{on} \ r = R_l, \tag{6}$$

$$\phi_m \mathbf{u}_m \cdot \mathbf{e}_r = \phi_c \mathbf{u}_c \cdot \mathbf{e}_r, \ \mathbf{e}_r \cdot \sigma_m \cdot \mathbf{e}_r = \mathbf{e}_r \cdot \sigma_c \cdot \mathbf{e}_r \ \text{on} \ r = R_m. \tag{7}$$

By (5), the normal stress condition on the membrane–cell layer interface is equivalent to continuity of pressure

$$p_m = p_c \quad \text{on} \ r = R_m. \tag{8}$$

On the moving outer boundary of the cell layer, $r = R_c(z, t)$, we impose continuity of the normal fluid velocity relative to the moving boundary

(i.e. conservation of mass) and continuity of normal stress

$$\phi_c \left(\mathbf{u}_c \cdot \mathbf{n}_c - \frac{\partial R_c}{\partial t} \right) = \mathbf{u}_e \cdot \mathbf{n}_c - \frac{\partial R_c}{\partial t},$$
$$\mathbf{n}_c \cdot \sigma_c \cdot \mathbf{n}_c = \mathbf{n}_c \cdot \sigma_e \cdot \mathbf{n}_c \quad \text{on} \ r = R_c(z, t), \tag{9}$$

where $\partial R_c/\partial t$ is given by the growth law prescribed in Eqs. (32) and (35) in Section 2.2.3, and $\mathbf{n}_c = (\mathbf{e}_r - \partial R_c/\partial z \ \mathbf{e}_z)/\sqrt{1 + (\partial R_c/\partial z)^2}$ is the outward-pointing unit normal to the cell layer boundary.

Flow of the culture medium past the permeable boundary of the membrane will cause a boundary layer to develop on the membrane surface in which the tangential fluid velocity is non-vanishing (Beavers and Joseph, 1967). This can be modelled using a Beavers–Joseph boundary condition (Shipley et al., 2010). However, following Shipley et al. (2010), who showed that the slip at the permeable boundary of the PLGA-PVA membrane has a negligible impact on the flow, we apply a no-slip boundary condition for the tangential component of the fluid velocity on $r = R_l$

$$\mathbf{u}_l \cdot \mathbf{e}_z = \phi_m \mathbf{u}_m \cdot \mathbf{e}_z \quad \text{on} \ r = R_l. \tag{10}$$

Similarly, we assume that the slip at the outer surface of the porous cell layer is negligible, and impose no slip there

$$\phi_c \mathbf{u}_c \cdot \mathbf{t}_c = \mathbf{u}_e \cdot \mathbf{t}_c \quad \text{on} \ r = R_c(z, t), \tag{11}$$

where $\mathbf{t}_c = (\partial R_c/\partial z \ \mathbf{e}_r + \mathbf{e}_z)/\sqrt{1 + (\partial R_c/\partial z)^2}$ is the tangent vector to the surface. To test the validity of this assumption the magnitude of the slip at the outer surface of the cell layer should be determined from measurements of the flow distribution with a cell layer attached to the hollow fibre. However, in the absence of such experimental data, we make the simplifying assumption that the cell layer permeability is low enough for (11) to provide a reasonable approximation to the Beavers–Joseph boundary condition.

We treat the ECS ports as being distributed over the entire curved wall of the ECS ($r = R_e$, $z \in [0, L]$), henceforth referred to as 'the ECS port', and set the fluid pressure to atmospheric pressure and the axial velocity to zero on this boundary

$$p_e = P_{atm}, \quad \mathbf{u}_e \cdot \mathbf{e}_z = 0 \quad \text{on } r = R_e. \tag{12}$$

Shipley et al. (2010) confirmed that this approach gives excellent agreement between model predictions and experimental measurements of the lumen and ECS flow rates when there is no cell layer, as the bulk of the pressure drop from the lumen to the ECS occurs across the membrane. Whilst the precise details of the flow in the cell layer and ECS will determine how closely the model predictions agree with experimental flow rate measurements when there is a growing cell layer, the membrane permeability will still be the key determinant of the flow in the ECS, since it is much lower than the cell layer permeability (see Table 1). Treating the ECS port as a distributed port should therefore still give a good approximation to explicitly modelling flow through the two ECS ports.

The ends of the fibre are glued into place with epoxy resin and the walls of the ECS are solid, so there is no flow out of the ends of the membrane, cell layer and ECS. Hence,

$$\mathbf{u}_m \cdot \mathbf{e}_z = \mathbf{u}_c \cdot \mathbf{e}_z = \mathbf{u}_e \cdot \mathbf{e}_z = 0 \quad \text{on } z = 0, L. \tag{13}$$

In the experimental set-up, the volumetric flow rate of fluid into the lumen and normal stress at the lumen outlet are fixed, so

$$2\pi \int_{r=0}^{R_l} r \mathbf{u}_l \cdot \mathbf{e}_z|_{z=0} \, \mathrm{d}r = Q_{l,in}, \tag{14}$$

$$\mathbf{e}_z \cdot \boldsymbol{\sigma}_l \cdot \mathbf{e}_z = P_{l,out} \quad \text{on } z = L, \, 0 < r < R_l. \tag{15}$$

These conditions are sufficient to determine the fluid pressures and velocities in the reduced model for the fluid flow obtained by exploiting the small aspect ratio of the bioreactor (see Appendices A and C).

2.2.2. Mass transport: oxygen and lactate

As the timescales for advection, diffusion and consumption of oxygen and production of lactate are much shorter than the timescale for cell layer growth for the flow rates we consider (see Section 3), we assume that the solute transport is quasi-steady on the growth timescale, and thus governed by steady advection–diffusion equations in the lumen and ECS

$$\nabla \cdot (c_i \mathbf{u}_i) = D_i \nabla^2 c_i \quad \text{for } i = l, e, \tag{16}$$

where c_i ($i = l, e$) is the solute (oxygen or lactate) concentration and D_i ($i = l, e$) are the assumed constant solute diffusivities in the lumen and ECS. In the membrane, the transport is governed by

$$\nabla \cdot (\phi_m c_m \mathbf{u}_m) = \nabla \cdot (\phi_m D_m \nabla c_m), \tag{17}$$

where c_m is the solute concentration (per unit volume of fluid) and D_m is the effective solute diffusivity (accounting for dispersion effects). In the cell layer, there is also oxygen uptake and lactate production, so the solute transport is described by the reaction–advection–diffusion equation

$$\nabla \cdot (\phi_c c_c \mathbf{u}_c) = \nabla \cdot (\phi_c D_c \nabla c_c) + m \phi_c \mathcal{R}(c_c), \tag{18}$$

where c_c is the solute concentration and D_c is the effective solute diffusivity, and the reaction term $m \phi_c \mathcal{R}(c_c)$ describes the rate of oxygen uptake (for $m = -1$) or lactate production (for $m=1$) by the cells. Eqs. (17) and (18) are derived by volume averaging (reaction-)advection–diffusion equations for the solute concentrations in the pore space over the membrane and cell layer, respectively (see Gray, 1975; Quintard and Whitaker, 1994 for further details).

Oxygen uptake by cell populations in HFBs is typically modelled by Michaelis–Menten kinetics (Abdullah and Das, 2007; Chen and Palmer, 2009; Das, 2007; Pillarella and Zydney, 1990; Shipley et al., 2011), for which

$$\mathcal{R}(c_c) = \frac{V_{max} c_c}{C_{1/2} + c_c}, \tag{19}$$

where V_{max} (in mol m^{-3} s^{-1}) is the maximal uptake rate per unit volume of the cell layer and $C_{1/2}$ is the concentration at which the uptake rate is half-maximal. Here we restrict attention to cell types for which $c_c \gg C_{1/2}$ (see Section 3), so that (19) can be approximated as constant

$$\mathcal{R}(c_c) \approx V_{max}, \tag{20}$$

and (18) can be solved analytically for a given position of the outer boundary of the cell layer, $r = R_c(z, t)$. We also assume that the lactate production rate is approximately constant, since the culture medium is sufficiently glucose-rich and the lactate concentration kept sufficiently low by lactate buffering for this to be a reasonable approximation (see Shipley and Waters, 2012).

Since the oxygen and lactate distributions are assumed to be axisymmetric, we impose no diffusive flux through $r=0$

$$D_l \nabla c_l \cdot \mathbf{e}_r = 0 \quad \text{on } r = 0. \tag{21}$$

At the lumen–membrane and membrane–cell layer interfaces we impose continuity of solute concentration and flux

$$c_l = c_m, \quad (c_l \mathbf{u}_l - D_l \nabla c_l) \cdot \mathbf{e}_r = \phi_m (c_m \mathbf{u}_m - D_m \nabla c_m) \cdot \mathbf{e}_r \quad \text{on } r = R_l, \tag{22}$$

$$c_m = c_c, \quad \phi_m (c_m \mathbf{u}_m - D_m \nabla c_m) \cdot \mathbf{e}_r = \phi_c (c_c \mathbf{u}_c - D_c \nabla c_c) \cdot \mathbf{e}_r, \quad \text{on } r = R_m. \tag{23}$$

At the outer surface of the cell layer we impose continuity of the concentration and flux relative to the moving boundary

$$c_m = c_c,$$
$$\phi_c c_c \left(\mathbf{u}_c \cdot \mathbf{n}_c - \frac{\partial R_c}{\partial t} \right) - \phi_c D_c \nabla c_c \cdot \mathbf{n}_c = (c_e \mathbf{u}_e - D_e \nabla c_e) \cdot \mathbf{n}_c \quad \text{on } r = R_c(z, t). \tag{24}$$

With the normal velocity continuity conditions in (6), (7) and (9), the flux conditions above reduce to continuity of diffusive flux

$$D_l \nabla c_l \cdot \mathbf{e}_r = \phi_m D_m \nabla c_m \cdot \mathbf{e}_r \quad \text{on } r = R_l, \tag{25}$$

$$\phi_m D_m \nabla c_m \cdot \mathbf{e}_r = \phi_c D_c \nabla c_c \cdot \mathbf{e}_r \quad \text{on } r = R_m, \tag{26}$$

$$\phi_c D_c \nabla c_c \cdot \mathbf{n}_c = D_e \nabla c_e \cdot \mathbf{n}_c \quad \text{on } r = R_c(z, t). \tag{27}$$

There is no concentration flux out of the ends of the membrane, cell-layer and ECS, so

$$D_i \nabla c_i \cdot \mathbf{e}_z = 0 \quad \text{on } z = 0, L \text{ for } i = m, c, e. \tag{28}$$

Experimentally, the oxygen concentration at the lumen inlet is held constant and there is no lactate in the culture medium entering the lumen, so

$$c_l = \begin{cases} C_{in} & \text{for oxygen,} \\ 0 & \text{for lactate,} \end{cases} \quad \text{on } z = 0, \, 0 < r < R_l. \tag{29}$$

Following Shipley and Waters (2012), we assume that the culture medium leaving the lumen outlet and ECS port is well-mixed and impose zero-diffusive-flux at these outlets for both the oxygen and lactate transport

$$D_l \nabla c_l \cdot \mathbf{e}_z = 0 \quad \text{on } z = L, \, 0 < r < R_l, \tag{30}$$

$$D_e \nabla c_e \cdot \mathbf{e}_r = 0 \quad \text{on } r = R_e. \tag{31}$$

2.2.3. Cell layer growth

We assume that the cell density in the cell layer is constant and that changes in the cell number occur at its outer surface, which moves outwards if the cell proliferation rate exceeds the cell death rate and inwards if the death rate exceeds the proliferation rate (due to cells that die detaching from the surface and being carried away by the flow). Cells in the bulk of the cell layer are assumed to be stationary and quiescent due to contact inhibition (Engel et al.,

Table 2
Cell culture, oxygen uptake, and lactate production parameter values for different cell types.

Solute	Cell type	Cell density (cells m^{-3})	C_{in} (mol m^{-3})	$C_{1/2}$ (mol m^{-3})	V_{max} (mol m^{-3} s^{-1})	Reference
Oxygen	Neonatal rat cardiomyocytes	10^{12}	0.22	6.9×10^{-3}	2.64×10^{-3}	Radisic et al. (2005)
	Primary rat hepatocytes		0.22	6.24×10^{-3}	1.76×10^{-3}	1.25×10^{13}	Sullivan et al. (2007)
	Pancreatic βTC3 cells		0.22	1.0×10^{-2}	2.8×10^{14}	6.37×10^{-3}	Tziampazis and Sambanis (1995), Stabler et al. (2009)
	Bovine chondrocytes	1.4×10^{14}	0.1	5.0×10^{-3}	4.8×10^{-5}	Malda et al. (2004), Obradovic et al. (1999), Fermor et al. (2007)
	Human foreskin fibroblasts (HFFs)	1.15×10^{-4}	0.19	2.1×10^{-3}	3.8×10^{12}	Korin et al. (2007)
Lactate	Rabbit articular chondrocytes (monolayer)			–	3.45×10^{-4}	Tomita et al. (2001)
	Bovine articular chondrocytes (3D culture)	1.4×10^{14}		–	1.32×10^{-5}	Obradovic et al. (1999)

C_{in}, $C_{1/2}$ and V_{max} as defined in Eqs. (29) and (19). Adapted from Shipley and Waters (2012).

2005; Machide et al., 2006; Lee et al., 2003; Guo et al., 1989).

Cell proliferation and death are assumed to depend on the oxygen and lactate concentrations, c and l, and interstitial fluid shear stress σ (the shear stress on the cells due to the flow through the spaces between the cells) at the surface of the cell layer. We assume that the growth depends on the interstitial shear stress rather than the shear stress on the cells from the ECS flow tangential to the surface, as the interstitial shear stress is an order of magnitude larger for the flow configuration considered here, both when the ECS ports are open and when they are closed. Thus the normal velocity of the outer surface of the cell layer is given by

$$\left(1 + \left(\frac{\partial R_c}{\partial z}\right)^2\right)^{-1/2} \frac{\partial R_c}{\partial t} = G(c, l, \sigma)|_{r=R_c(z,t)}, \tag{32}$$

where the growth function G is to be prescribed. We note that this model is equivalent to the thin-rim (fast-consumption) limit of a two-phase free-boundary model for the cells and culture medium in which fast nutrient consumption at the tissue surface prevents nutrient transport to the tissue interior so that cell proliferation is consigned to the free boundary (King and Franks, 2006), except that in the present model growth in the cell layer interior is prevented by contact inhibition rather than lack of nutrients.

We estimate the interstitial shear stress from the interstitial fluid velocity by assuming that the flow through the interstitial spaces can be approximated as Poiseuille flow through a circular duct of diameter d with mean velocity $|\mathbf{u}_c|$. With $\tilde{r}$ as the local radial coordinate, the interstitial velocity profile is therefore

$$u_p \approx 2|\mathbf{u}_c|\left(1 - 4\frac{\tilde{r}^2}{d^2}\right), \tag{33}$$

so the interstitial shear stress on the cells is

$$\sigma = \mu\left|\frac{\partial u_p}{\partial \tilde{r}}\right|_{\tilde{r}=d/2} \approx \frac{16\mu|\mathbf{u}_c|\tilde{r}}{d^2}\bigg|_{\tilde{r}=d/2} = \frac{8\mu|\mathbf{u}_c|}{d}. \tag{34}$$

Following previous studies (McElwain and Ponzo, 1977; Jones et al., 2000; Lewis et al., 2005), and based on experimental evidence that the proliferation rate of many cell types increases with oxygen availability (Wang et al., 2005; Kim et al., 2001; Murrell et al., 1990), we assume that the cell proliferation rate increases linearly with the oxygen concentration provided it exceeds the minimum threshold required for proliferation, C_{min}. As data on the relationships between cell death and lactate concentration, and cell death and shear stress, is more limited, we assume that cells die and detach from the cell layer surface at a constant rate when either the lactate concentration exceeds the threshold at which it is toxic to the cells, L_{max}, and/or the shear stress exceeds a critical threshold, Σ_d. The effects of excess lactate and shear stress are taken to be multiplicative, so that cells die at a faster

rate when both $l > L_{max}$ and $\sigma > \Sigma_d$. We use a smoothed Heaviside function rather than a normal Heaviside function to describe the lactate and shear stress effects as l and σ cross L_{max} and Σ_d, as a normal Heaviside function would lead to discontinuities in $\partial R_c/\partial t$ and very sharp changes in $R_c(z, t)$ that would be difficult to resolve numerically and for which the reduced model derived in the small aspect ratio limit (Appendix A) would not be valid. Since the cell layer stops growing if it fills the entire ECS or recedes to the fibre surface (which is taken to represent all the cells dying), $R_m \leq R_c(z, t) \leq R_e$. Thus we arrive at the following form for G

$$G(c, l, \sigma) = [A_p(c - C_{min})\mathrm{H}(c - C_{min})\mathrm{F}(\Sigma_d - \sigma, s_s)$$
$$-B_d[(1 + B_L\mathrm{F}(l - L_{max}, s_L))(1 + B_s\mathrm{F}(\sigma - \Sigma_d, s_s)) - 1]] \tag{35}$$

where $\mathrm{H}(\cdot)$ is the Heaviside function and $\mathrm{F}(x, s) = \frac{1}{2}(1 + \tanh(sx))$ is the smoothed Heaviside function with smoothing factor s; the constant A_p is the growth rate of the cell layer per unit concentration if $c > C_{min}$ and there is no cell death ($l < L_{max}$ and $\sigma < \Sigma_d$); and B_d, B_L and B_s together determine the recession rate of the cell layer if $l > L_{max}$ and/or $\sigma > \Sigma_d$ and there is no cell proliferation ($c < C_{min}$ or $\sigma > \Sigma_d$).

Finally, we prescribe the initial depth of the cell layer as a function of z

$$R_c(z, 0) = R_{c,init}(z). \tag{36}$$

The full model for the flow, solute transport and cell layer growth is thus given by Eqs. (2)–(32) and (34)–(36).

3. Model parameterisation and reduction

Typical values of the model parameters are given in Tables 1–3. Where parameters are not obtainable from the literature, we determine them via physical arguments in Appendix B. We nondimensionalise Eqs. (2)–(36) and exploit the small aspect ratio of the bioreactor to simplify the system (see Appendix A for details). For the inlet flow rates in Table 1, the reduced Reynolds number for the flow (the ratio of inertial to viscous forces in the fluid), $\epsilon^2 Re = \epsilon^2 \rho UL/\mu$, is in the range 5.3×10^{-3}–5.3×10^{-2} (i.e. viscous forces in the fluid dominate inertial forces), so we are justified in neglecting inertia in the lumen and ECS flow equations (2). The reduced Péclet numbers in the different regions (the ratios of the rates of axial advection to those of radial diffusion), $\epsilon^2 Pe_i = \epsilon^2 UL/D_i$ ($i = l, m, c, e$), are all $O(1)$, so advection and diffusion are equally important. Although the maximum oxygen uptake/lactate production rate, V_{max}, is cell-type dependent (see Table 2), we assume that the dimensionless uptake/production rate is $O(1)$ to retain a balance between the rates of uptake/production and diffusion in the reduced model, thus keeping our analysis as general as possible. We estimate the cell layer growth rate per unit concentration, A_p, for different cell types (Table 3) from their cell doubling times (see

Table 3
Cell layer growth parameter values.

Cell type	A_P (µm h⁻¹/(mol m⁻³))	B_d (µm h⁻¹)	C_{min} (mol m⁻³)	L_{max} (mol m⁻³)	Σ_d (Pa)	References
Neonatal rat cardiomyocytes	2.3	0.5	6×10^{-3}–8×10^{-2}	0.4	0.03	Takamiya et al. (2011), Korin et al. (2007)
Primary rat hepatocytes	2.3	0.5	2.1×10^{-2}	0.4	2	Davidson et al. (2010), Nyberg et al. (1994)
Pancreatic βTC3 cells	–	–	1.46×10^{-2}	0.4	1.4	Tziampazis and Sambanis (1995), Stabler et al. (2009), Sankar et al. (2011)
Bovine chondrocytes	1.8	0.2	2.2×10^{-3}–1.32×10^{-2}	0.4	2	Galban and Locke (1997), Whittaker et al. (2009)
HFFs	12.1	2.3	2.1×10^{-2}	0.4	0.03	Korin et al. (2007)

A_P, B_d, C_{min}, L_{max} and Σ_d as defined in Eq. (35). See Appendix B for explanation of how A_P is estimated. Weight factors for cell layer recession rate for excess lactate and excess shear stress, B_L and B_s, taken to be 1 in all simulations. Smoothing factors for lactate and shear-stress dependence functions in (35) chosen as $s_s = 10^5$ and $s_L = 10$.

Appendix B.2). Since the cell layer growth timescale is much longer than the timescales for advection and solute diffusion, we are justified in assuming that the flow and solute transport are quasi-steady on the growth timescale (see Appendix B.2).

In our simulations we vary seven parameters to determine their effect on the cell layer growth: the lumen inlet flow rate $Q_{l,in}$, the lumen outlet pressure $P_{l,out}$, the maximum oxygen uptake/lactate production rate, V_{max}, the growth rate A_P, and the oxygen and lactate concentration thresholds and shear stress threshold for cell proliferation and death, C_{min}, L_{max} and Σ_d. In the absence of experimental data for the concentration at which lactate becomes toxic to the cells, L_{max}, we follow Whittaker et al. (2009) and fix $L_{max} = 0.4$ mol m⁻³ as a default value for all cell types in our simulations.

Full details of how the reduced equations governing the cell layer growth ((A.2)–(A.26) in Appendix A) are solved are given in Appendix C. Briefly, we integrate the fluid and solute transport equations (2)–(3) and (16)–(18), over the depth of each region to derive a PDE for the lumen pressure (C.4) and expressions for the fluid pressures, flow velocities and solute concentrations in each region in terms of the lumen pressure (C.7)–(C.18). The coupled flow, solute transport and cell layer growth problem is then solved numerically for a given starting position of the outer surface of the cell layer. At each time step, the lumen pressure PDE is solved for the current position of the outer surface of the cell layer and the solution used to update the flow velocities, solute concentrations and position of the outer surface of the cell layer according to the growth law (32).

4. Results

4.1. Flow profiles and oxygen and lactate distributions

4.1.1. Uniform vs non-uniform cell layer depth

Before simulating the cell layer growth, we compared the flow, and oxygen and lactate distributions in layers of rat cardiomyocytes of fixed uniform and non-uniform depths to assess the impact of non-uniformity in the depth on oxygen delivery to, and lactate removal from, the cells. Variations in the cell layer depth can arise experimentally from non-uniformity in the initial cell seeding on the surface of the fibre or in the subsequent cell proliferation, or both. Fig. E1 in Appendix E shows that the uniformity of the cell layer depth has little effect on the fluid pressure distribution, and therefore the flow profiles (Fig. E2), in the bioreactor. This is because the majority of the pressure drop from the lumen to the ECS occurs across the membrane and not the more permeable cell layer. However, the uniformity of the cell layer can have a significant effect on the oxygen and lactate distributions. For example, changing from a constant cell layer depth to one that decreases linearly along the fibre (but keeping the volume of the cell layer the same), switches the minimum oxygen and maximum lactate concentrations from being at the ECS wall around the lumen outlet

($r \in [R_c, R_e]$, $z=L$) (Figs. E3(a) and E4(a)) to the ECS wall around the lumen inlet ($r \in [R_c(0), R_e]$, $z=0$) (Figs. E3(b) and E4(b)). This is because more oxygen is taken up and more lactate produced where the cell layer is thicker, since the number of cells in the cross-section of the cell layer is greater (as the cell density is assumed constant). The sensitivity of the solute distributions to the uniformity of the cell layer depth suggests that fine control over the culture conditions may be required to maintain uniform solute distributions, and hence uniform growth, for cells with high nutrient demands.

4.1.2. Changes in flow profiles and solute distributions with growth

The cell layer grows outwards from the fibre provided that the shear stress is below the threshold at which cells die ($\sigma|_{r=R_c} < \Sigma_d$), there is sufficient oxygen ($c|_{r=R_c} > C_{min}$), and either the lactate concentration is below the threshold at which it causes cell death ($l|_{r=R_c} < L_{max}$) or the positive effect of oxygen on growth outweighs the negative effect of lactate. As the cell layer grows, the surface oxygen concentration $c|_{r=R_c}$ decreases and the surface lactate concentration $l|_{r=R_c}$ increases, causing growth to slow over time. If $l|_{r=R_c} < L_{max}$ and $c|_{r=R_c}$ decreases to C_{min} (or $c|_{r=R_c} > C_{min}$ and $l|_{r=R_c} > L_{max}$) and the positive and negative effects of oxygen and lactate on the growth balance each other, then the cell layer attains a steady state depth. Since the radial flow velocity in the ECS decreases with r (as shown in Fig. E2b), the shear stress on the cells at the outer surface decreases as the layer grows. Hence, if $\sigma|_{r=R_c}$ is initially below Σ_d, it will remain so as the cell layer grows (see Fig. 4(c)). Conversely, if $\sigma|_{r=R_c}$ is initially above Σ_d, then the cell layer recedes and the shear stress on the surface cells increases. Hence, the layer will continue to recede until it reaches the fibre surface (see Figs. 5 and 6, which are discussed in detail in Section 4.2.1).

4.2. Cell layer growth simulations

For sustained growth of the cell layer it is required that $c|_{r=R_c} > C_{min}$, $l|_{r=R_c} < L_{max}$, and $\sigma|_{r=R_c} < \Sigma_d$. In this investigation we assume that the bioreactor dimensions and membrane properties (its depth and permeability) are fixed, and that our control parameters are $Q_{l,in}$ and $P_{l,out}$ and the initial depth of the cell layer ($R_{c,init}(z) - R_m$), as these are the parameters that can be readily prescribed experimentally. As the governing equations for the flow, solute transport and cell layer growth must be solved numerically, it is not possible to define analytical operating equations for $Q_{l,in}$ and $P_{l,out}$ based on the conditions on c, l and σ as in Shipley et al. (2011) and Shipley and Waters (2012). Instead, we perform numerical simulations to compare the growth of cell types with different oxygen demands and shear stress tolerances for flow rates and outlet pressures typical of those used in experiments: $Q_{l,in} \in [3.33 \times 10^{-9}$ m³ s⁻¹, 3.33×10^{-8} m³ s⁻¹] and $P_{l,out} \in [1.027 \times 10^5$ Pa, 2.068×10^5 Pa]. We consider two cell types: rat cardiomyocytes, which have high oxygen requirements (max-

imum oxygen uptake rate $V_{max}^O = 2.64 \times 10^{-3}\,\text{mol m}^{-3}\,\text{s}^{-1}$, $C_{min} = 8 \times 10^{-2}\,\text{mol m}^{-3}$) and are assumed to have low shear stress tolerance $(\Sigma_d = 0.03\,\text{Pa})$, and bovine chondrocytes, - which have low oxygen requirements ($V_{max}^O = 4.8 \times 10^{-5}\,\text{mol m}^{-3}\,\text{s}^{-1}$, $C_{min} = 5 \times 10^{-3}\,\text{mol m}^{-3}$) and can withstand higher shear stresses $(\Sigma_d = 2\,\text{Pa})$. We assume that initially the cells form a layer of uniform depth 50 μm (i.e. approximately 5 cells deep) along the length of the fibre, so that $R_c(z, 0) = R_{c,init}(z) = 450\,\mu\text{m}$. The simulations enable us to predict values of $Q_{l,in}$ and $P_{l,out}$ that maximise the average depth to which the cell layer grows in a set time or minimise the time it takes to grow to fill the ECS. We also briefly consider the impact of variation in the initial cell layer depth with z on the cell layer growth, and the sensitivity of the growth to the lactate toxicity threshold, L_{max}.

The simulations are run for a maximum period of $T=60$ days, or until a stopping criterion is reached (the cell layer grows to fill the entire ECS, recedes to the fibre surface or reaches a steady state). A maximum culture time of 60 days is chosen since significant degradation of the PLGA in the membrane occurs for longer times (Hoque et al., 2012; Azimi et al., 2014), increasing the membrane permeability and invalidating our assumption that it remains constant. Once 60 days have elapsed, the mean and standard deviation of the final outer radius of the cell layer, $\overline{R}_c = \frac{1}{L}\int_0^L R_c(z, T)\,\text{d}z$ and $\text{SD} = \sqrt{\frac{1}{L}\int_0^L (R_c(z, T) - \overline{R}_c)^2\,\text{d}z}$, are recorded.

4.2.1. Impact of flow rate and outlet pressure on growth

The oxygen and lactate concentrations and shear stress at the outer surface of the cell layer, and hence the growth rate of the cell layer, depend on $Q_{l,in}$ and $P_{l,out}$. Figs. 3(a) and (b) show how $\overline{R}_c$ varies with $Q_{l,in}$ and $P_{l,out}$ for cardiomyocytes and chondrocytes respectively.

The cell layer fails to fill the ECS (which would correspond to $\overline{R}_c = 1000\,\mu\text{m}$) in 60 days for either cell type for any of the flow rates and outlet pressures considered. However for the cardiomyocytes, $\overline{R}_c$ attains its maximum value, 871 μm, when $Q_{l,in} = 3.33 \times 10^{-8}\,\text{m}^3\,\text{s}^{-1}$ and $P_{l,out} = 1.965 \times 10^5\,\text{Pa}$ (shown by the green circle in Fig. 3(a)), and decreases sharply when $P_{l,out} > 1.965 \times 10^5\,\text{Pa}$ (to the right of the vertical green line in Fig. 3(a)). This change is due to the changes in the balance of the effects of increased oxygen concentration and

increased shear stress at the surface of the cell layer as $Q_{l,in}$ and $P_{l,out}$ increase ($l \ll L_{max}$ for both cell types over the range of flow rates and outlet pressures considered). For $P_{l,out} < 1.965 \times 10^5\,\text{Pa}$, the shear stress σ is below the cell death threshold, $\Sigma_d = 0.03\,\text{Pa}$, over the whole length of the fibre, so no cell death occurs (Fig. 4), and cell proliferation increases as $Q_{l,in}$ and $P_{l,out}$ increase due to improved oxygen delivery. For $P_{l,out} > 1.965 \times 10^5\,\text{Pa}$, as $P_{l,out}$ increases σ exceeds Σ_d over an increasing length of the fibre, so cells die and the cell layer recedes towards the fibre surface at $r = 400\,\mu\text{m}$ (Fig. 5). For chondrocytes, $\overline{R}_c$ increases monotonically as $Q_{l,in}$ and $P_{l,out}$ increase, since the shear stress is much lower than the threshold at which they die, $\Sigma_d = 2\,\text{Pa}$.

Our model predicts that the growth rate of the cardiomyocyte layer is maximised if we fix the flow rate and outlet pressure to be $Q_{l,in} = 3.33 \times 10^{-8}\,\text{m}^3\,\text{s}^{-1}$ and $P_{l,out} = 1.965 \times 10^5\,\text{Pa}$; for the chondrocytes the growth rate is maximised when $Q_{l,in} = 3.33 \times 10^{-8}\,\text{m}^3\,\text{s}^{-1}$ and $P_{l,out} = 2.068 \times 10^5\,\text{Pa}$ (green circle in Fig. 3(b)).

For the cardiomyocytes, the standard deviation in the outer radius of the cell layer at $t=60$ days, SD, decreases as $Q_{l,in}$ decreases and as $P_{l,out}$ increases for $P_{l,out} < 1.931 \times 10^5\,\text{Pa}$, ranging from 0.2 μm (when $Q_{l,in} = 2 \times 10^{-8}\,\text{m}^3\,\text{s}^{-1}$ and $P_{l,out} = 1.931 \times 10^5\,\text{Pa}$) to 44 μm (when $Q_{l,in} = 3.33 \times 10^{-8}\,\text{m}^3\,\text{s}^{-1}$ and $P_{l,out} = 1.034 \times 10^5\,\text{Pa}$). For the chondrocytes, SD also decreases as $Q_{l,in}$ decreases and $P_{l,out}$ increases, but is much smaller than for the cardiomyocytes for each combination of $Q_{l,in}$ and $P_{l,out}$, $\text{SD} = 0–2\,\mu\text{m}$. The greater variation in the depth of the cell layer for the cardiomyocytes is due to their greater oxygen uptake rate. Their greater uptake rate means that at low outlet pressures increasing the flow rate only increases oxygen delivery to the upstream end of the cell layer, so it grows more quickly than the downstream end.

4.2.2. Impact of variation in initial cell layer depth on growth

In the previous simulations the initial depths of the cell layers were uniform along the fibre. However, since the oxygen and lactate distributions are affected by the degree of uniformity of the cell layer, variation in its initial depth along the fibre can significantly affect its subsequent growth. Such variation in the cell layer depth often arises as a result of spatial heterogeneity in the cell seeding distribution, so in this section we explore its potential impact on the growth of the cell layer.

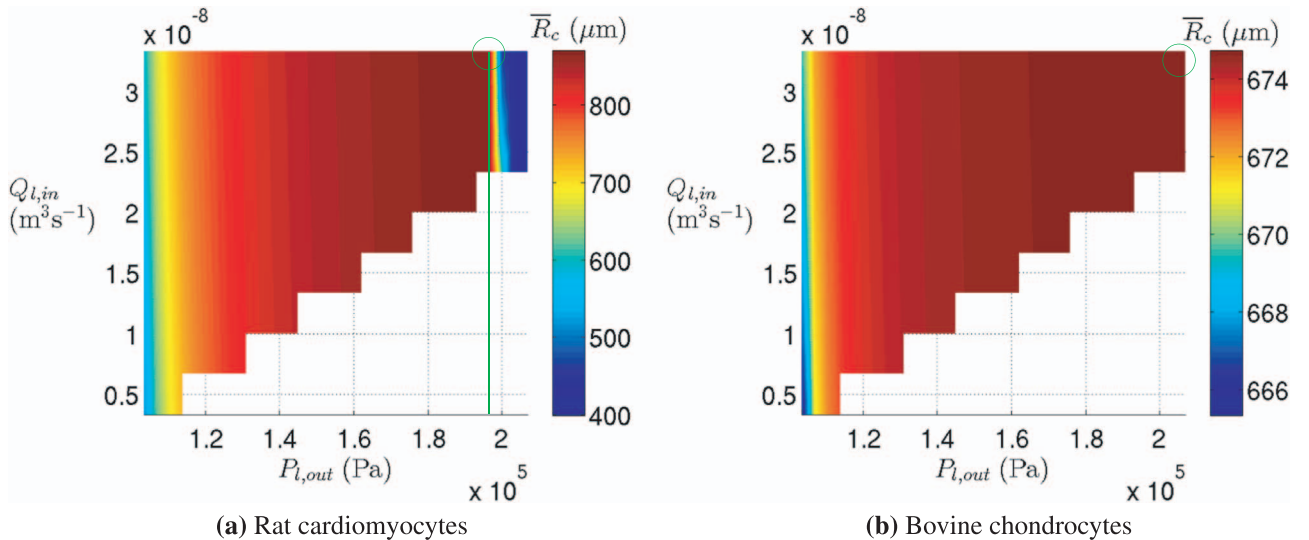We simulate the growth of the layer of rat cardiomyocytes described

(a) Rat cardiomyocytes   **(b) Bovine chondrocytes**

Fig. 3. Contour plots showing how $\overline{R}_c$, the mean outer radius of the cell layer at $t=60$ days, depends on the lumen inlet flow rate $Q_{l,in}$ and lumen outlet pressure $P_{l,out}$ for (a) rat cardiomyocytes and (b) bovine chondrocytes, when the ECS port is open. Standard deviation in the cell layer depth at $t=60$ days: (a) SD = 0.2–44 μm (b) SD = 0–2 μm. The reduced model for the flow, solute transport and cell layer growth (Eqs. (A.24)–(A.26) and (C.4)–(C.18) in Appendices A and C) corresponding to Eqs. (2)–(36) was solved with $R_{c,init}(z) = 450\,\mu\text{m}$. Parameter values: (a) $V_{max}^O = 2.64 \times 10^{-3}\,\text{mol m}^{-3}\,\text{s}^{-1}$, $V_{max}^L = 1.32 \times 10^{-3}\,\text{mol m}^{-3}\,\text{s}^{-1}$, $C_{min} = 8 \times 10^{-2}\,\text{mol m}^{-3}$, $L_{max} = 0.4\,\text{mol m}^{-3}$, $\Sigma_d = 0.03\,\text{Pa}$, (b) $V_{max}^O = 4.8 \times 10^{-5}\,\text{mol m}^{-3}\,\text{s}^{-1}$, $V_{max}^L = 1.32 \times 10^{-5}\,\text{mol m}^{-3}\,\text{s}^{-1}$, $C_{min} = 1.32 \times 10^{-2}\,\text{mol m}^{-3}$, $L_{max} = 0.4\,\text{mol m}^{-3}$, $\Sigma_d = 2\,\text{Pa}$. All other parameter values as in Tables 1–3. Green circles mark the values of $Q_{l,in}$ and $P_{l,out}$ at which $\overline{R}_c$ is maximised. Vertical green line in (a) shows the outlet pressure above which recession of the cell layer occurs, $P_{l,out} = 1.965 \times 10^5\,\text{Pa}$, since $\sigma > \Sigma_d$. White region corresponds to outlet pressures at which there is backflow at the lumen outlet for the given inlet flow rate. (See online version of paper for colour version of this figure.)
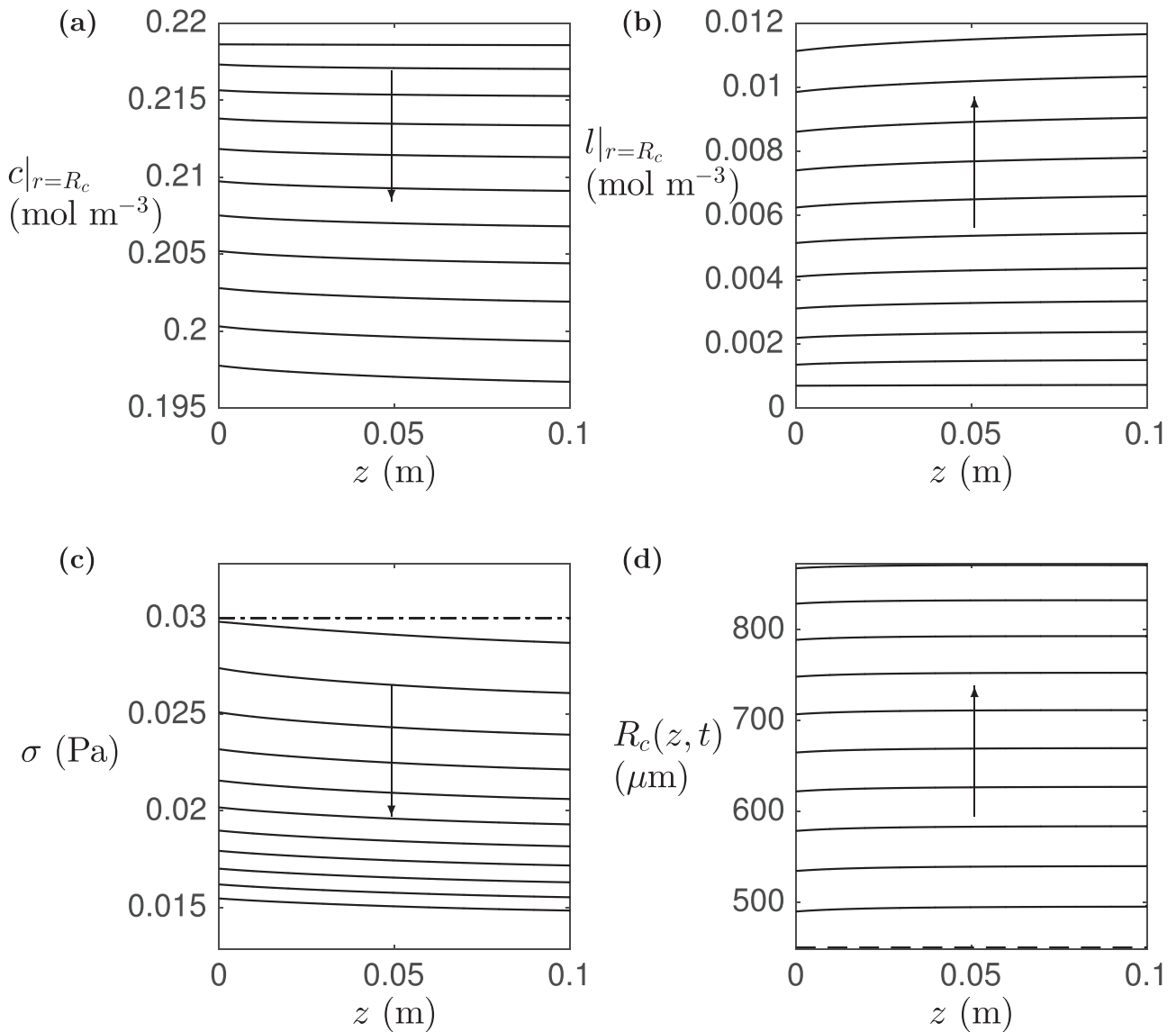
Fig. 4. Evolution of (a) the surface oxygen concentration $c|_{r=R_c}$, (b) surface lactate concentration $l|_{r=R_c}$, (c) surface interstitial shear stress $\sigma|_{r=R_c}$ and (d) outer surface $r = R_c(z, t)$ of a layer of rat cardiomyocytes. Mean and standard deviation of outer radius at t=60 days: $\bar{R}_c = 871\ \mu m$, SD = 3 μm. Initial cell layer depth and parameter values as in Fig. 3(a) with $Q_{l,in} = 3.33 \times 10^{-8}\ m^3\ s^{-1}$, $P_{l,out} = 1.965 \times 10^5$ Pa. Arrows indicate direction of increasing time, solid lines the dependent variables at regular intervals of 6 days, dash-dot line in (c) the shear stress cell death threshold Σ_d, and dashed line in (d) the initial cell layer outer radius $R_{c,init}(z) = 450\ \mu m$.

in Section 4.1.1, whose depth decreases linearly along the fibre (as a simple example of a non-uniform cell layer), at the flow rate and outlet pressure predicted to be optimal for the growth of the uniform layer in Section 4.2.1 ($Q_{l,in} = 3.33 \times 10^{-8}\ m^2\ s^{-1}$ and $P_{l,out} = 1.965 \times 10^5$ Pa). We obtain a very different result from Fig. 4, as shown in Fig. 6. Since the non-uniform cell layer is initially thinner at its downstream end, the shear stress on the cells at the surface is higher than for the uniform layer and exceeds Σ_d. Hence the cell layer quickly recedes towards the fibre surface at its downstream end (for $z > 7.38$ cm), but grows outwards over the upstream part of the fibre ($z < 7.36$ cm) (Fig. 6(d)), where $\sigma < \Sigma_d$ (Fig. 6(c)). The shear stress on the cells at the downstream end increases as the cell layer recedes, so the layer continues to recede until it reaches the membrane at $r = 400\ \mu m$ after 5 days. Consequently, after 60 days the mean final outer radius of the cell layer, $\bar{R}_c = 750\ \mu m$ is much smaller (and the standard deviation in the final outer radius, SD = 211 μm, much larger) than for the initially uniform cell layer with the same flow rate and outlet pressure. Whilst the change in the depth of the cell layer between $z = 7.36$ cm and $z = 7.38$ cm in Fig. 6(d) appears sharp, it should be noted that the cell

layer is less than 0.5 mm deep, so the gradient of the surface in this region is of order 1. Nevertheless, the change in depth may be sharper than would occur in practice, and reflects the simplicity of the form of shear stress dependence assumed in the cell layer growth law (35).

Reducing $P_{l,out}$ brings the shear stress on the cells near the outlet below Σ_d, so that the cell layer grows outwards over its whole length to a mean outer radius of $\bar{R}_c = 870\ \mu m$ after 60 days. However, the cell layer remains thicker at its upstream end and the standard deviation in the final outer radius (SD = 16 μm) is larger than for the uniform cell layer. Similar results are observed when the initial depth of the cell layer *increases* with z ($R_c(z, 0) = R_{c,init}(z) = (419 + 6.\ 1 \times 10^{-4}\ z)\ \mu m$)— the cell layer recedes at the downstream end—(where $\sigma > \Sigma_d$) if $Q_{l,in} = 3.33 \times 10^{-8}\ m^3\ s^{-1}$ and $P_{l,out} = 1.965 \times 10^5$ Pa, so that $\bar{R}_c = 705\ \mu m$ and SD = 14 μm, but grows over its whole length at lower outlet pressures.

5. Comparison with flow, solute transport and growth with ECS port closed

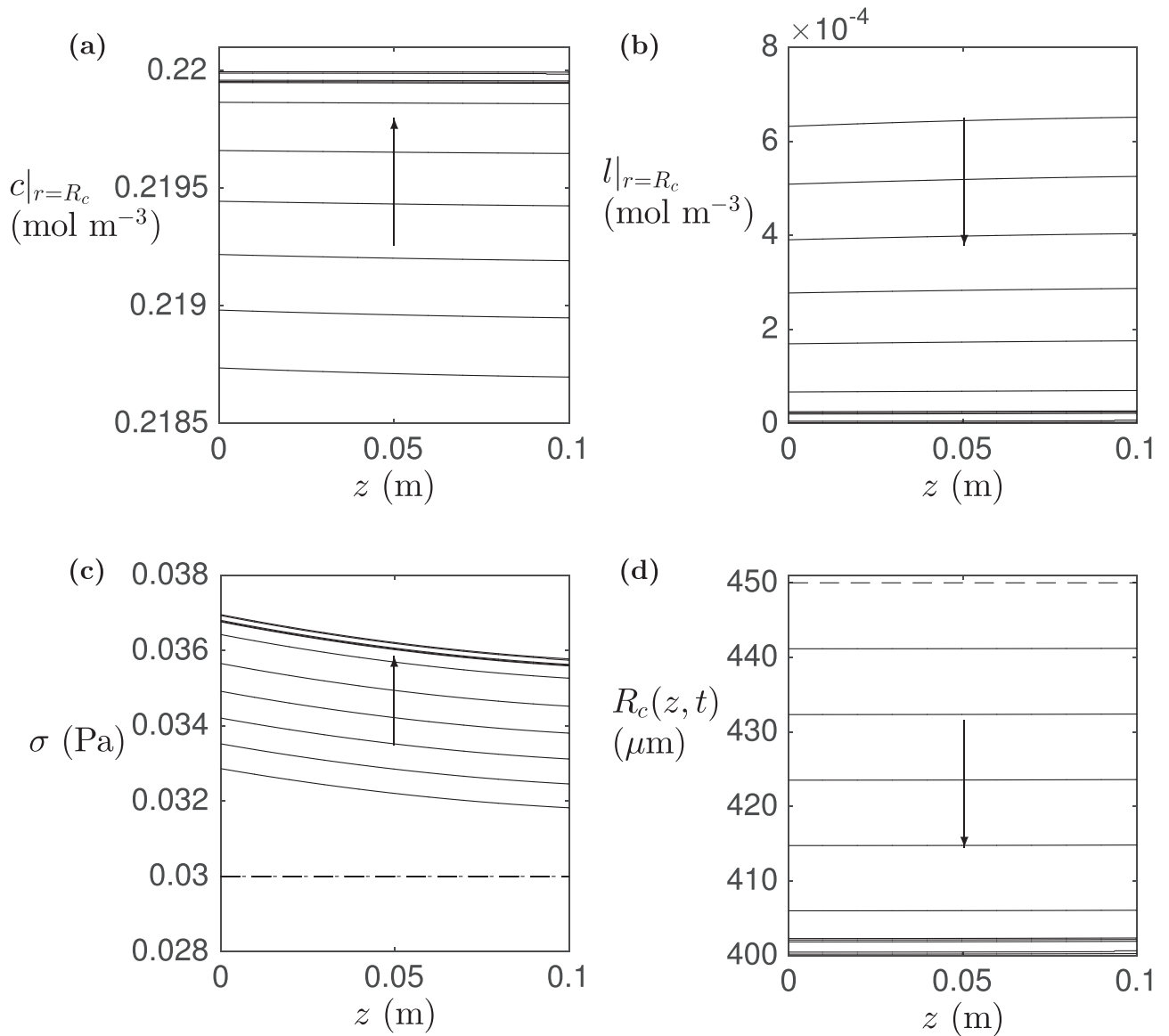Finally we briefly describe the key differences in the flow, solute

Fig. 5. Evolution of (a) $c|_{r=R_c}$, (b) $l|_{r=R_c}$, (c) $\sigma|_{r=R_c}$ and (d) $R_c(z, t)$ for a layer of rat cardiomyocytes with too high an outlet pressure. Cell layer in (d) recedes to fibre surface at $r = 400$ μm. Parameter values as in Fig. 4 with $Q_{l,in} = 3.33 \times 10^{-8}$ m^3 s^{-1}, $P_{l,out} = 2.068 \times 10^5$ Pa. Lines and arrows as in Fig. 4.

transport and cell layer growth when the ECS port is closed.

5.1. Flow

When the ECS port is closed, there is no normal flow out of, or axial flow along, the ECS outer boundary,

$$\mathbf{u}_e \cdot \mathbf{e}_r = 0, \quad \mathbf{u}_e \cdot \mathbf{e}_z = 0 \text{ on } r = R_e, \tag{37}$$

so the axial flow in the lumen dominates the radial flow and flow is negligible in the rest of the bioreactor (see Appendix D.1). For the cell types and range of flow rates considered here, the interstitial shear stress remains far below the cell death threshold, Σ_d. Thus changes in the interstitial shear stress due to changes in $Q_{l,in}$ and $P_{l,out}$ do not affect the growth of the cell layer.

5.2. Solute transport

As before, we nondimensionalise the governing equations ((2)–(13), (14)–(36), (37)) and exploit the small aspect ratio of the bioreactor to simplify the resulting system as in Appendix A. The mass transport problem for the oxygen and lactate reduces to solving an advection–diffusion equation for the lumen concentration at each growth time step (see Appendix D.2). Since radial flow through the bioreactor is much weaker than when the ECS port is open, the rates at which oxygen is transported through the membrane to the cells and lactate is advected away from the cell layer are much lower. Consequently the minimum oxygen and maximum lactate concentrations are much lower and higher respectively. For example, for the uniform cell layer in Fig. 4(d) ($R_c = 450$ μm) the minimum oxygen concentration with the ECS port closed is 0.108 mol m^{-3} (compared to 0.216 mol m^{-3} with the port open) and the maximum lactate concentration is 0.119 mol m^{-3} (more than 60 times higher than with the port open).

With the ECS port closed, the leading order oxygen and lactate concentrations at the outer surface of the cell layer, and therefore the cell layer growth rate, depend on $Q_{l,in}$ (through its effect on the oxygen and lactate transport through the lumen) but not on $P_{l,out}$. As when the ECS port is open, the growth rate of the cell layer decreases as it grows out into the ECS, since the surface oxygen concentration decreases with distance from the fibre. Since cell layer growth does not affect the dominant flow in the bioreactor, it only affects the oxygen and lactate distributions by altering uptake/production and diffusion within the
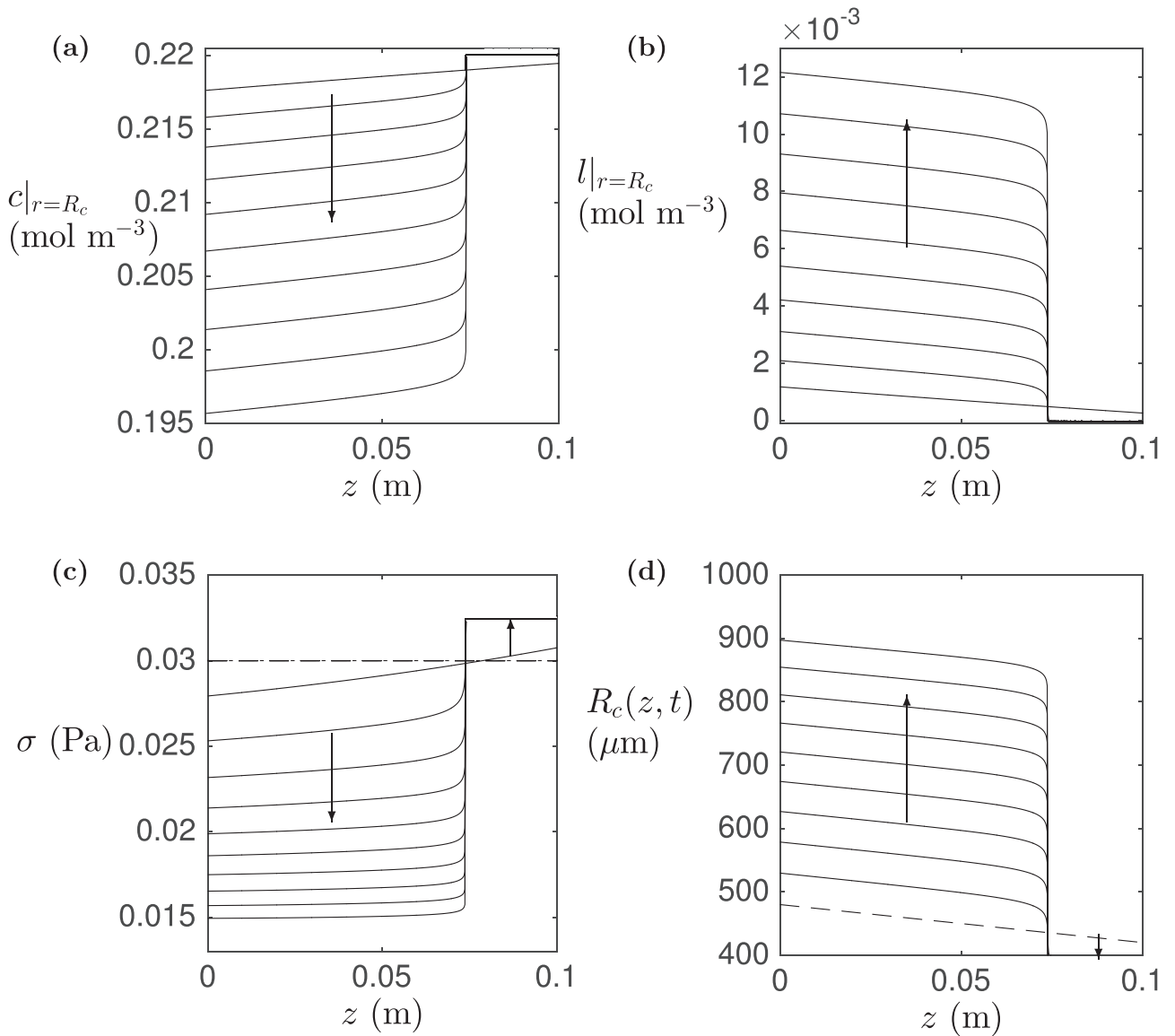
Fig. 6. Evolution of (a) $c|_{r=R_c}$, (b) $l|_{r=R_c}$, (c) $\sigma|_{r=R_c}$ and (d) $R_c(z, t)$ for an initially non-uniform layer of rat cardiomyocytes. Cell layer grows outwards at upstream end ($z < 7.36$ cm), but recedes to fibre surface in 5 days at downstream end ($z > 7.38$ cm) (d) where $\sigma > \Sigma_d$ (c). Note the scales on the axes, from which it can be seen that the gradient of the surface between the regions of growth and recession is of order 1. Initial cell layer outer radius $R_{c,init}(z) = (480 - 6.\ 1 \times 10^{-4}\ z)$ μm. Mean outer radius at t=60 days, $\overline{R}_c = 750$ μm. Parameter values as in Fig. 4 ($Q_{l,in} = 3.33 \times 10^{-8}$ m³ s⁻¹, $P_{l,out} = 1.965 \times 10^5$ Pa). Lines and arrows as in Fig. 4.

ECS (it changes the latter as the solutes diffuse more slowly in the cell layer than in the free fluid in the ECS).

5.3. Growth

The reduced system for the flow, solute transport and growth with the ECS port closed is solved as described in Appendix D.3, and used to simulate the growth of initially uniform layers of rat cardiomyocytes and bovine chondrocytes as in Section 4.2.1. Fig. 7 shows how $\overline{R}_c$, the mean outer radius of the cell layer at t=60 days, varies with $Q_{l,in}$ for the cardiomyocytes and chondrocytes ($R_{c,init}(z) = 450$ μm as in Fig. 3). The cardiomyocyte layer quickly reaches a steady state depth ($\overline{R}_c = 463$–466 μm), since the surface oxygen concentration $c_{l,r=R_c}$ rapidly approaches C_{min}. By contrast, the depth of the chondrocyte layer has not reached equilibrium after 60 days, when $\overline{R}_c = 656$–657 μm. In this case the oxygen uptake rate is lower, so $c_{l,r=R_c}$ remains well above C_{min} as the cell layer grows. For both cardiomyocytes and chondrocytes lactate levels remain below the threshold for cell death, $L_{max} = 0.4$ mol m⁻³, throughout the simulation period.

The cardiomyocyte layer grows far less than when the ECS port is open ($\overline{R}_c = 463$–466 μm compared to 516–871 μm when $P_{l,out} < 1.965 \times 10^5$ Pa), whereas the reduction in growth is very small for the chondrocyte layer ($\overline{R}_c = 656$–657 μm compared to 665–675 μm). The reduction in growth when the ECS port is closed is due to reduced radial flow and oxygen delivery to the cells. The effect is more pronounced for the cardiomyocytes as they consume oxygen at a higher rate, causing the oxygen concentration at the outer surface of the cell layer to decrease more rapidly as it grows.

Fig. 7 shows that increasing $Q_{l,in}$ has only a modest effect on the final cell layer depth for both cardiomyocytes and chondrocytes. This is because increasing $Q_{l,in}$ increases only advective transport through the lumen at leading order when the ECS port is closed, leading to a marginal increase in the oxygen concentration at the inner surface of the membrane, which propagates through the membrane and cell layer by diffusion. The variation in the cell layer depth at t=60 days for the cardiomyocytes is much smaller when the ECS port is closed (SD = 0.5–1.4 μm) than when it is open (SD = 0.2–44 μm), as expected given that the cardiomyocyte layer grows very slowly. The reduction is

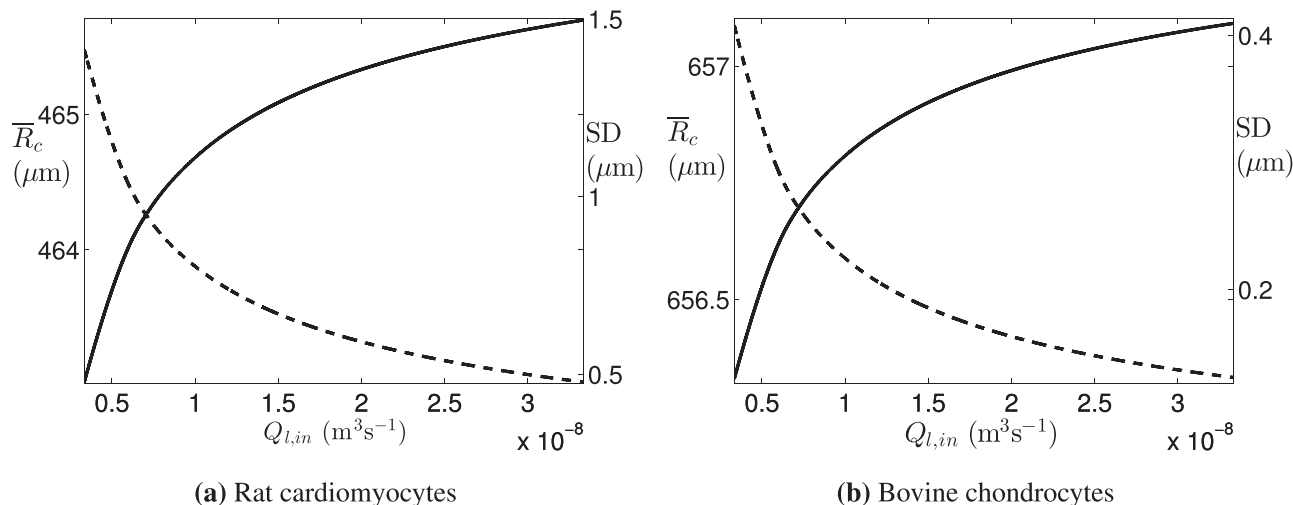**(a)** Rat cardiomyocytes

(b) Bovine chondrocytes

Fig. 7. Variation in the mean, $\overline{R}_c$, and standard deviation, SD, of the cell layer outer radius at t=60 days with $Q_{l,in}$ for (a) rat cardiomyocytes and (b) bovine chondrocytes, when the ECS port is closed. Parameter values: (a) as in Fig. 3(a); (b) as in Fig. 3(b). Solid line shows $\overline{R}_c$, dashed line SD.

less pronounced for the chondrocytes (SD = 0.1–0.4 μm compared to SD = 0–2 μm).

From these results it is clear that opening the ECS port and using higher flow rates and outlet pressures can enhance cell layer growth. However, it is important to know the level of shear stress that the cells can withstand.

5.4. Sensitivity of growth to lactate concentration

So far, we have assumed that the lactate concentration at which cell death occurs is the same for all cells (L_{max} = 0.4 mol m^{-3}), and have found that for the cell types and operating conditions considered the lactate concentration at the outer surface of the cell layer remains much lower than L_{max}. In the absence of cell-type-specific data for L_{max}, the sensitivity of the cell layer growth to L_{max} warrants further investigation. Therefore we now simulate the growth of an initially uniform rat cardiomyocyte layer as L_{max} varies in the range 0.001–0.4 mol m^{-3}. Fig. 8 shows how the growth of the cell layer (measured as the difference, $\overline{\Delta R_c}$, between its mean final outer radius, $\overline{R}_c$, and initial outer radius, $R_{c,init}$ = 450 μm) varies with L_{max} when the ECS port is closed and when it is open. With the ECS port closed, the cell layer

recedes if $L_{max} < 0.14$ mol m^{-3} (i.e. if L_{max} is to the left of the vertical line in Fig. 8(a)), the recession increasing as L_{max} decreases, but grows if $L_{max} > 0.14$ mol m^{-3}. For $L_{max} > 0.25$ mol m^{-3}, growth is approximately constant. With the ECS port open, the cell layer grows even for low values of L_{max}, the amount of growth increasing as L_{max} increases until $L_{max} = 0.15$ mol m^{-3}. For $L_{max} > 0.15$ mol m^{-3} growth does not change with L_{max}. The fact that growth is more sensitive to the value of L_{max} when the ECS port is closed, and that the cell layer may recede if L_{max} is low, further underlines the benefits of operating the bioreactor with the ECS port open.

6. Discussion

The simulation results show that opening the ECS ports, increasing $Q_{l,in}$ and increasing $P_{l,out}$ all improve growth, provided that the shear stress on the cells at the surface does not exceed that at which the cells die or detach from the layer (both processes being captured by recession of the cell layer in the model). Our results also show that the improvement in growth associated with opening the ECS ports is greater for cells with higher oxygen demands (Fig. 3).

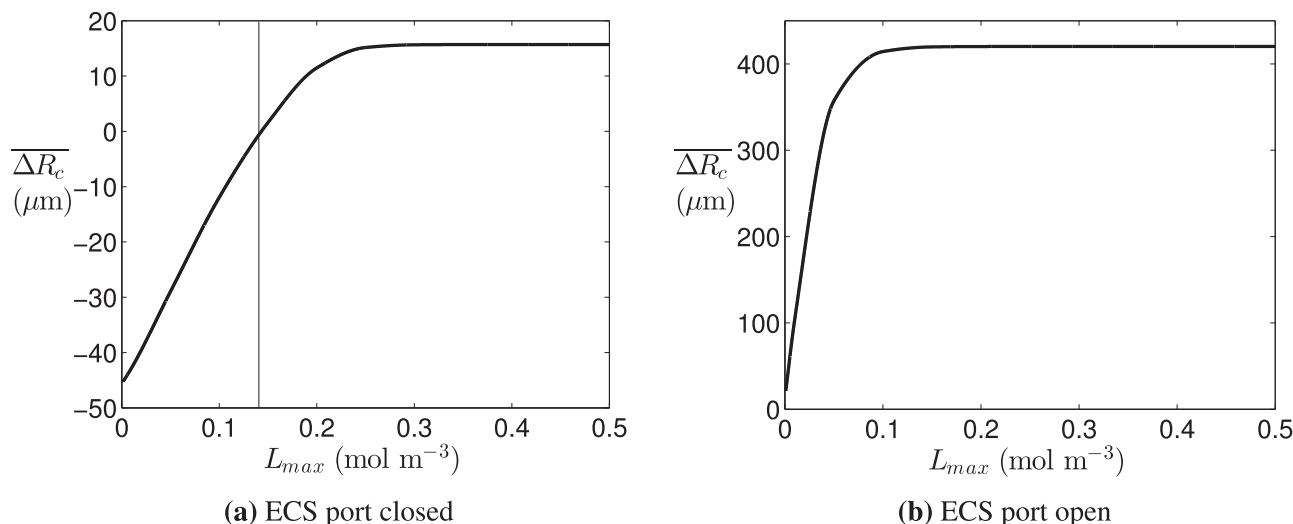Increasing $Q_{l,in}$ and/or $P_{l,out}$ increases the oxygen concentration and

(a) ECS port closed

(b) ECS port open

Fig. 8. Variation in the growth of a rat cardiomyocyte cell layer with the lactate cell death threshold L_{max} after 60 days of culture with the ECS port (a) closed and (b) open. Vertical line in (a) shows minimum lactate threshold for cell layer growth, $L_{max} = 0.14$ mol m^{-3}, for given operating conditions. Initial cell layer outer radius $R_{c,init}(z) = 450$ μm. Cell layer growth measured by $\overline{\Delta R_c} = \overline{R}_c - R_{c,init}$. Parameter values as in Fig. 4.

decreases the lactate concentration at the cell layer surface, but also increases the shear stress on the cells. For shear-sensitive cells it is necessary to avoid imposing too high an outlet pressure and inlet flow rate. In view of this, we have used the model to predict the inlet flow rate and outlet pressure that maximise the growth of initially uniform layers of rat cardiomyocytes (assumed to be shear-sensitive) and bovine chondrocytes (shear-tolerant) when the ECS ports are open, and have predicted a lower optimal $P_{l,out}$ for rat cardiomyocytes (Fig. 3). This highlights the extent to which the optimal flow rate and outlet pressure will be cell-type-specific. Cells should be cultured at the highest possible $Q_{l,in}$ and $P_{l,out}$ for which the interstitial shear stress in the cell layer remains below Σ_d, to maximise oxygen delivery and lactate clearance.

Although our model simulations predict that cells such as cardiomyocytes, with high oxygen demands (high V_{max}^O and C_{min}), should be grown with the ECS ports open, it may be better to keep the ECS ports closed for cells that are very sensitive to shear stress (have a very low Σ_d) or have sufficiently low oxygen requirements that the culture medium can be recycled directly from the outlet to the inlet (i.e. does not need to be replaced) without any adverse effect on the growth. When the ECS port is open, the predicted percentage increase in the cell number for an initially uniform layer of cardiomyocytes is 1300% after 60 days (for $Q_{l,in} = 3.33 \times 10^{-8}$ m^3 s^{-1} and $P_{l,out} = 1.965 \times 10^5$ Pa), based on the volume change of the cell layer and assuming that the cells are all spherical with a fixed radius of 10 μm (Table B1), while for chondrocytes it is 600% (for $Q_{l,in} = 3.33 \times 10^{-8}$ m^3 s^{-1} and $P_{l,out} = 2.068 \times 10^5$ Pa). When the ECS port is closed, the percentage increases in cell number for cardiomyocytes and chondrocytes are 30% and 500% respectively (for $Q_{l,in} = 3.33 \times 10^{-8}$ m^3 s^{-1}). We anticipate that opening the ECS port and using a high flow rate and outlet pressure could lead to similar improvements in growth for rat hepatocytes and pancreatic beta cells to those for rat cardiomyocytes, given their similar oxygen requirements and higher shear stress tolerances (Tables 2 and 3).

For the cell types we have considered, the surface lactate concentration remains well below the estimated toxicity threshold, L_{max}, for typical operating conditions (see Figs. 4–6), and oxygen is the growth-rate limiting solute. However, in the absence of experimental estimates of L_{max}, we have used the model to predict the sensitivity of the cell layer growth to L_{max}. Our results suggest that the range of values of L_{max} for which the lactate concentration is growth-rate limiting (or causes recession of the cell layer) is smaller when the ECS ports are open. Therefore it may be better for the ECS ports to be open if L_{max} is not known for the cell type being cultured (provided the cells are not highly shear-sensitive).

Our simulations demonstrate that cell layer growth (and the optimal flow rate and outlet pressure) may be sensitive to variation in the initial cell layer depth along the fibre (Fig. 6). They predict that the cell layer will grow less and have a less uniform depth after 60 days if its initial depth is non-uniform. This suggests that cell seeding and initial culture conditions should be aimed at producing a uniform cell layer depth (by making the initial cell density on the fibre surface and the solute distributions as uniform as possible) to maximise growth and the uniformity of the final cell layer. However, in practice it can be difficult to achieve such uniformity in the initial cell density and therefore in the growth (Chapman et al., 2014). We have considered initial cell layers, $r = R_{c,init}(z)$, whose depth is uniform or decreases/increases linearly with distance along the fibre as an initial exploration of the impact of non-uniformity on the cell layer growth. However, further investigation of choices for $R_{c,init}(z)$ is needed to confirm whether non-uniformity has only a negative impact on the growth.

Simulating growth with different $R_{c,init}(z)$ across a range of experimental values of $Q_{l,in}$ and $P_{l,out}$ would also enable the prediction of optimal combinations of $R_{c,init}(z)$, $Q_{l,in}$ and $P_{l,out}$.

There are several ways in which this study could be extended and the accuracy of its predictions improved. The first step would be to validate the model predictions against experiments for specific cell types. This would involve estimating parameters such as the lactate toxicity threshold L_{max} and shear stress death threshold Σ_d, and the death rates under excess lactate and shear stress, $B_L B_d$ and $B_s B_d$. It may be necessary to use a more detailed growth law to capture the precise dependence of the proliferation and death rates on the oxygen and lactate concentrations.

Although contact inhibition is believed to be significant for the cell types considered here, it would be instructive to consider simulations in which growth occurs throughout the cell layer, rather than just at the free surface, to see how the growth predictions differ. An assessment of which assumption is more realistic, i.e. surface or volumetric growth, could then be made by comparing model predictions to experimental measurements of cell layer growth.

A simplifying assumption made in deriving the model was that the cell layer is initially axisymmetric and remains so as it grows. In practice, there will be some azimuthal variation in the cell layer depth, and this may affect cell layer growth. However, to include such variation in the model would require fully 3D simulations, which would be highly computationally expensive, and hence lie beyond the scope of this study.

Further possible extensions include using a multiphase description of the cell layer to account for variation in the cell layer porosity with time due to cell proliferation and extra-cellular matrix deposition (Pearson et al., 2015b), and using a more detailed model of cell metabolism incorporating glucose and protein transport (Shipley et al., 2009) and coupling between the oxygen, glucose and lactate concentrations (Casciari et al., 1992).

7. Conclusions

We have developed a model of cell layer growth in a single-fibre HFB by extending a previous HFB fluid and mass transport model (Shipley and Waters, 2012). Our model incorporates dependence of cell layer growth on local oxygen and lactate concentrations and on local fluid shear stress. This enables predictions to be made of the effect of varying the lumen inlet flow rate and lumen outlet pressure on the growth of different cell types. We have observed that opening the ECS ports and increasing the flow rate and outlet pressure enhance growth for shear-tolerant cells by increasing oxygen delivery, but that it may be necessary to use lower outlet pressures for shear-sensitive cells to maximise growth.

Once parameterised against experimental data, our model could be used to make quantitative predictions of the optimal operating conditions for different cell types.

Acknowledgements

Appendix A. Nondimensionalisation

We nondimensionalise Eqs. (2)–(36) for the fluid transport, oxygen and lactate transport and cell layer growth with the following scalings:

$$r = R_l \hat{r}, \quad z = L\hat{z}, \quad t = \frac{R_l}{A_p C_{in}}\hat{t}, \ u_{i,r} = \epsilon U \hat{u}_{i,r}, \quad u_{i,z} = U\hat{u}_{i,z}, \quad p_i = P_{atm} + P_i \hat{p}_i, \ \sigma_i = P_i \hat{\sigma}_i, \quad c_i = \begin{cases} C_{in}\hat{c}_i & \text{for oxygen,} \\ C_L \hat{c}_i & \text{for lactate,} \end{cases} \quad i = l, m, c, e, \ \sigma = P_c \hat{\sigma},$$

$$G(c, l, \sigma) = A_p C_{in} \widehat{G}(\hat{c}_O, \hat{c}_L, \hat{\sigma}), \ R_c(z, t) = R_l \widehat{R}_c(\hat{z}, \hat{t}), \quad R_{c,init}(z) = R_l \widehat{R}_{c,init}(\hat{z}), \tag{A.1}$$

where $U = Q_{l,in}/(2\pi R_l^2)$ is a typical lumen flow velocity; $P_l = \mu U/(\epsilon^2 L)$, $P_i = \mu\epsilon U R_l/k_i$ $(i = m, c)$, $P_e = \mu U/L$ are the pressure scales in the different regions; and C_L is a typical lactate concentration. We then exploit the small aspect ratio of the bioreactor to neglect terms at leading order in $\epsilon = R_l/L \ll 1$. From here on we omit hats on dimensionless variables.

The mass conservation and radial and axial momentum conservation equations in the lumen and ECS in (2) become

$$\frac{\partial p_l}{\partial r} = 0, \quad \frac{1}{r}\frac{\partial}{\partial r}\left(r\frac{\partial u_{l,z}}{\partial r}\right) = \frac{\partial p_l}{\partial z}, \quad \frac{1}{r}\frac{\partial}{\partial r}(ru_{l,r}) + \frac{\partial u_{l,z}}{\partial z} = 0, \tag{A.2}$$

$$\phi_i u_{i,r} = -\frac{\partial p_i}{\partial r}, \quad u_{i,z} = 0, \quad \frac{\partial}{\partial r}\left(r\frac{\partial p_i}{\partial r}\right) = 0, \ i = m, c, \tag{A.3}$$

$$\frac{1}{r}\frac{\partial}{\partial r}\left(r\frac{\partial u_{e,r}}{\partial r}\right) - \frac{u_{e,r}}{r^2} = \frac{\partial p_e}{\partial r}, \quad \frac{\partial}{\partial r}\left(r\frac{\partial u_{e,z}}{\partial r}\right) = 0, \ \frac{1}{r}\frac{\partial}{\partial r}(ru_{e,r}) + \frac{\partial u_{e,z}}{\partial z} = 0, \tag{A.4}$$

so there is no axial flow in the membrane or cell layer at leading order.

In dimensionless coordinates the lumen–membrane and membrane–cell layer interfaces, cell layer outer surface and ECS outer boundary are given by $r=1$, $r = R_m/R_l =: \widehat{R}_m$, $r = \widehat{R}_c(z, t)$ and $r = R_e/R_l =: \widehat{R}_e$ respectively. The dimensionless continuity conditions at the lumen–membrane and membrane–cell layer interfaces are

$$u_{l,r} = -\frac{\partial p_m}{\partial r} \quad \text{and} \quad p_l = \kappa_m p_m \text{ on } r = 1, \tag{A.5}$$

$$\frac{\partial p_m}{\partial r} = \frac{\partial p_c}{\partial r} \quad \text{and} \quad p_m = \kappa_c p_c \text{ on } r = \widehat{R}_m, \tag{A.6}$$

where $\kappa_m := \epsilon^2 R_l^2/k_m$ is a dimensionless parameter representing the permeability of the membrane and $\kappa_c := k_m/k_c$ is the ratio of the membrane and cell layer permeabilities. Both κ_m and κ_c are assumed to be $O(1)$ to retain as many physical effects as possible at leading order.

At the moving surface of the cell layer, the normal velocity continuity condition in (9) becomes

$$\phi_c u_{c,r} = u_{e,r} - \frac{\partial \widehat{R}_c}{\partial z}u_{e,z} \quad \text{on } r = \widehat{R}_c(z, t), \tag{A.7}$$

where we have neglected the contribution from the cell layer growth, $(1 - \phi_c)(L/U)/(R_l A_p/C_{in})\frac{\partial \widehat{R}_c}{\partial t}$, on the left-hand side since the advection timescale L/U is much shorter than the growth timescale $R_l/(A_p C_{in})$ (see Appendix B.2), and also the $-\phi_c \frac{\partial \widehat{R}_c}{\partial z}u_{c,z}$ component of the normal velocity on the left-hand side since $u_{c,z} = O(\epsilon^2)$.

The normal stress condition at the moving boundary of the cell layer reduces to

$$p_c = 0 \quad \text{on } r = \widehat{R}_c(z, t). \tag{A.8}$$

The no-slip conditions at the lumen–membrane interface and the moving boundary, (10) and (11), reduce to

$$u_{l,z} = 0 \quad \text{on } r = 1, \tag{A.9}$$

$$u_{e,z} = 0 \quad \text{on } r = \widehat{R}_c(z, t). \tag{A.10}$$

At the outer boundary of the ECS, the dimensionless boundary conditions are

$$p_e = 0, \quad u_{e,z} = 0 \text{ on } r = \widehat{R}_e. \tag{A.11}$$

The dimensionless lumen inlet flow rate and outlet pressure are

$$\int_{r=0}^{1} ru_{l,z}|_{z=0} \, \mathrm{d}r = 1, \tag{A.12}$$

$$p_l = \widehat{P}_{l,out} \quad \text{on } z = 1, \ 0 < r < 1. \tag{A.13}$$

The advection–diffusion equations in the lumen, membrane and ECS, (16) and (17), and the reaction–advection–diffusion equation in the cell layer (18) become

$$\epsilon^2 Pe_i\left(\frac{1}{r}\frac{\partial}{\partial r}(rc_i u_{i,r}) + \frac{\partial}{\partial z}(c_i u_{i,z})\right) = \frac{1}{r}\frac{\partial}{\partial r}\left(r\frac{\partial c_i}{\partial r}\right), \quad i = l, e, \tag{A.14}$$

$$\epsilon^2 Pe_m \frac{1}{r}\frac{\partial}{\partial r}(rc_m u_{m,r}) = \frac{1}{r}\frac{\partial}{\partial r}\left(r\frac{\partial c_m}{\partial r}\right), \tag{A.15}$$

$$\epsilon^2 Pe_c \frac{1}{r} \frac{\partial}{\partial r}(rc_c u_{c,r}) = \frac{1}{r} \frac{\partial}{\partial r}\left(r \frac{\partial c_c}{\partial r}\right) + m\mathcal{M},$$

(A.16)

where $\epsilon^2 Pe_i := \epsilon^2 UL/D_i$ $(i = l, m, c, e)$ are the reduced Péclet numbers for the different regions, and $\mathcal{M} := V^O_{max} R_l^2/(C_{in} D_c^O)$ and $\mathcal{M} := V^L_{max} R_l^2/(C_L D_c^L)$ are the dimensionless oxygen uptake and lactate production rates respectively (the ratio of the rates of uptake/production to that of radial diffusion of the solute).

The dimensionless zero-diffusive-flux condition on the lumen axis is

$$\frac{\partial c_l}{\partial r} = 0 \quad \text{on } r = 0.$$

(A.17)

The dimensionless concentration and diffusive flux continuity conditions at the interfaces between the different regions are

$$c_l = c_m, \quad \frac{\partial c_l}{\partial r} = \frac{\phi_m D_m}{D_l} \frac{\partial c_m}{\partial r} \quad \text{on } r = 1,$$

(A.18)

$$c_m = c_c, \quad \frac{\partial c_m}{\partial r} = \frac{\phi_c D_c}{\phi_m D_m} \frac{\partial c_c}{\partial r} \quad \text{on } r = \widehat{R}_m,$$

(A.19)

$$c_c = c_e, \quad \frac{\partial c_c}{\partial r} = \frac{D_e}{\phi_c D_c} \frac{\partial c_e}{\partial r} \quad \text{on } r = \widehat{R}_c(z, t).$$

(A.20)

The dimensionless inlet concentration is

$$c_l = \begin{cases} 1 & \text{for oxygen,} \\ 0 & \text{for lactate,} \end{cases} \quad \text{on } z = 0, \, 0 < r < 1,$$

(A.21)

and the zero-diffusive flux conditions at the lumen outlet and outer boundary of the ECS are

$$\frac{\partial c_l}{\partial z} = 0 \quad \text{on } z = 1, \, 0 < r < 1,$$

(A.22)

$$\frac{\partial c_e}{\partial r} = 0 \quad \text{on } r = \widehat{R}_e.$$

(A.23)

The dimensionless form of the cell layer growth law (32) is

$$\frac{\partial \widehat{R}_c}{\partial t} = \widehat{G}\left(c|_{r=\widehat{R}_c}, \, l|_{r=\widehat{R}_c}, \, \sigma|_{r=\widehat{R}_c}\right),$$

(A.24)

where

$$\widehat{G}(c, l, \sigma) = [\text{H}(c - c_{min})(c - c_{min})\text{F}(\sigma_d - \sigma) - [\beta_L \text{F}(l - l_{max}) + \beta_s \text{F}(\sigma - \sigma_d) + \beta_{L,s}\text{F}(l - l_{max})\text{F}(\sigma - \sigma_d)]] \times \text{H}(\widehat{R}_c - \widehat{R}_m)\text{H}(\widehat{R}_e - \widehat{R}_c),$$

(A.25)

and $\sigma = \kappa_s|u_{c,r}|$ is now the dimensionless interstitial shear stress in the cell layer with proportionality constant $\kappa_s = 8k_c/(R_l d)$; and $c_{min} = C_{min}/C_{in}$ and $l_{max} = L_{max}/C_L$ are the dimensionless minimum oxygen and maximum lactate concentrations for cell proliferation; $\sigma_d = k_c \Sigma_d/(\mu \epsilon U R_l)$ is the dimensionless shear stress threshold for cell death/detachment; and $\beta_L = B_L B_d/(A_p C_{in})$, $\beta_s = B_s B_d/(A_p C_{in})$ and $\beta_{L,s} = B_L B_s B_d/(A_p C_{in})$ are the ratios of the cell layer recession rates due to excess lactate and excess shear stress, and the two combined, to the cell proliferation rate.

The initial condition for the position of the outer surface of the cell layer becomes

$$\widehat{R}_c(z, 0) = \widehat{R}_{c,init}(z).$$

(A.26)

Appendix B. Parameter estimates

B.1. Cell layer permeability

The permeability of the cell layer, k_c, is very difficult to measure experimentally and varies significantly with the initial seeding density and cell type. Assuming that the cell layer is densely packed with cells, we can estimate its permeability from its porosity ϕ_c and the average cell radius d_{cell} using the Kozeny–Carman equation (Kozeny, 1927; Carman, 1937)

$$k_c = \frac{\phi_c^3}{(1 - \phi_c)^2} \frac{d_{cell}^2}{180}.$$

(B.1)

For a porosity of $\phi_c = 0.6$ (Shipley and Waters, 2012) and a typical cell diameter of $d_{cell} = 10\,\mu\text{m}$, (B.1) gives $k_c \approx 7.5 \times 10^{-13}\,\text{m}^2$, which agrees

Table B1
Cell doubling time T_d and estimated cell layer growth rate per unit oxygen concentration A_p for different cell types.

Cell type	d_{cell} (μm)	T_d (h)	$A_p = d_{cell}/(C_{in}T_d)$ (μm h^{-1}(mol m^{-3})$^{-1}$)	Reference
Neonatal rat cardiomyocytes	10	20	2.3	Takamiya et al. (2011)
Primary rat hepatocytes	10	20	2.3	Davidson et al. (2010) and Nyberg et al. (1994)
Bovine chondrocytes	10	56	1.8	Galban and Locke (1997) and Whittaker et al. (2009)
HFFs	40	17	12.1	Korin et al. (2007)

reasonably well with the range of values 10^{-12}–10^{-8} used in other studies (Heath et al., 1990; Hay et al., 2001).

B.2. Cell layer growth rate

We estimate the growth rate of the cell layer per unit concentration, A_p, for different cell types from their cell doubling times (see Table B1). As we have assumed that only the outermost layer of cells in the cell region proliferates, we can assume that in the absence of cell death the depth of the cell region will increase by approximately one cell diameter d_{cell} in the cell doubling time T_d, so that

$$A_p \approx \frac{d_{cell}}{C_{in} T_d}. \tag{B.2}$$

Estimates for A_p for different cell types are given in Table B1. For simplicity we assume that the baseline recession rate of the cell layer due to cell death and detachment from excess lactate or shear stress, B_d, is the same as the rate at which the cell layer grows due to cell proliferation, $A_p C_{in}$, and the dimensionless weights for the excess lactate and shear stress recession rates, B_L and B_s, are both 1, so that $\beta_L = B_L B_d/(A_p C_{in}) = 1$, $\beta_s = B_s B_d/(A_p C_{in}) = 1$, and $\beta_{L,s} = B_L B_s B_d/(A_p C_{in}) = 1$.

For the cell types in Table B1 the cell layer growth timescale $R_l/(A_p C_{in})$ is $\sim 10^5$ s, whereas the advection timescale L/U is in the range 0.75–7.5 s for the flow rates in Table 1, and the timescales for radial diffusion and uptake/production of oxygen and lactate are in the ranges 13–290 s and 30–3000 s respectively. Hence, we are justified in assuming that the fluid and mass transport equations (2) and (16)–(18) are quasi-steady on the growth timescale.

B.3. Shear stress parameters

To estimate the dimensionless shear stress constant, $\kappa_s = 8k_c/(R_l d)$, we need to estimate the size d of the interstitial spaces in the cell layer. Using the empirical relationship for the permeability of a membrane and the average pore diameter derived by Bear (1988)

$$k_c = Cd^2, \tag{B.3}$$

where $C = 6.54 \times 10^{-4}$, and our estimate for k_c from Appendix B.1 (7.5×10^{-13} m^2) gives $d \approx \sqrt{k_c/C} = 3.4 \times 10^{-5}$ m, so $\kappa_s \approx 8.9 \times 10^{-4}$. The maximum shear stress that the cells can withstand without dying or detaching from the surface of the cell layer, Σ_d, depends on the cell type. While bovine chondrocytes grow well under shear stresses of up to 2 Pa (Smith et al., 1995), rat cardimyocytes can be damaged or killed by shear stresses higher than 0.16 Pa (Radisic et al., 2005). The level of shear stress that cells can withstand generally decreases (from order 1 Pa to order 0.1 Pa and smaller) as the length of time that they are exposed to it increases (Chapman et al., 2014, Supporting Information, Table S6). Studies with human foreskin fibroblasts (HFFs) and mouse osteoblasts in micro-channel bioreactors have shown that cell detachment can occur at shear stresses as low as 0.03 Pa (Korin et al., 2007; Leclerc et al., 2006). To incorporate the possibility of thinning of the cell layer due to cell detachment, we use values of Σ_d, appropriate to the cell types we consider, in the range 0.03–2 Pa.

Appendix C. Solution of the reduced model

Integrating the lumen, membrane and cell layer flow equations (A.2)–(A.3) with respect to r and applying the boundary conditions (A.5)–(A.6), (A.9)–(A.10) gives

$$p_l = p_l(z, t), \quad u_{l,r} = \frac{1}{16} \frac{\partial^2 p_l}{\partial z^2} r(2 - r^2), \; u_{l,z} = -\frac{1}{4} \frac{\partial p_l}{\partial z}(1 - r^2), \tag{C.1}$$

$$p_m = \frac{p_l}{\kappa_m} - \frac{1}{16} \frac{\partial^2 p_l}{\partial z^2} \ln r, \quad u_{m,r} = \frac{1}{16\phi_m} \frac{\partial^2 p_l}{\partial z^2} \frac{1}{r}, \tag{C.2}$$

$$p_c = \frac{p_l}{\kappa_c \kappa_m} - \frac{1}{16} \frac{\partial^2 p_l}{\partial z^2} \left(\ln r + \left(\frac{1}{\kappa_c} - 1 \right) \ln \widehat{R}_m \right), \; u_{c,r} = \frac{1}{16\phi_c} \frac{\partial^2 p_l}{\partial z^2} \frac{1}{r} \tag{C.3}$$

Applying (A.8) then gives a second order PDE for the lumen pressure

$$\frac{\partial^2 p_l}{\partial z^2} - \lambda^2 p_l = 0, \tag{C.4}$$

where

$$\lambda(z, t) = \sqrt{\frac{16}{\kappa_m (\kappa_c \ln \widehat{R}_c(z, t) + (1 - \kappa_c) \ln \widehat{R}_m)}}, \tag{C.5}$$

with boundary conditions (from (A.12) and (A.13))

$$\frac{\partial p_l}{\partial z}(0, t) = -16, \quad p_l(1, t) = \widehat{P}_{l,out}. \tag{C.6}$$

Using (C.4) and integrating the ECS flow equations (A.4) subject to the boundary conditions (A.7) and (A.11), the fluid pressures and radial flow velocities simplify to

$$p_m = \frac{1}{\kappa_m} \left(1 - \frac{\lambda(z, t)^2}{16} \kappa_m \ln r \right) p_l, \tag{C.7}$$

$$p_c = \frac{1}{\kappa_c \kappa_m} \left(1 - \frac{\lambda^2}{16} \kappa_m (\kappa_c \ln r + (1 - \kappa_c) \ln \widehat{R}_m) \right) p_l,$$

(C.8)

$$p_e = 0, \quad u_{l,r} = \frac{\lambda^2 p_l}{16} r (2 - r^2), \quad u_{m,r} = \frac{\lambda^2 p_l}{16 \phi_m r},$$

(C.9)

$$u_{c,r} = \frac{\lambda^2 p_l}{16 \phi_c r}, \quad u_{e,r} = \frac{\lambda^2 p_l}{16 r}.$$

(C.10)

Substituting these and (C.1) into the solute transport equations (A.14)–(A.16), integrating with respect to r subject to the boundary conditions (A.17)–(A.23) gives

$$c_l(r, z, t) = \begin{cases} 1 & \text{for oxygen,} \\ 0 & \text{for lactate,} \end{cases}$$

(C.11)

$$c_i(r, z, t) = A_i(z, t) + B_i(z, t) r^{n_i(z,t)} \quad \text{for } i = m, e,$$

(C.12)

$$c_c(r, z, t) = A_c(z, t) + B_c(z, t) r^{n_c(z,t)} + \frac{m\mathcal{M}}{2(n_c(z, t) - 2)} r^2,$$

(C.13)

$$c_e(r, z, t) = A_c(z, t) + B_c(z, t) \widehat{R}_c^{n_c} + \frac{m\mathcal{M} \widehat{R}_c^2}{2(n_c - 2)},$$

(C.14)

where

$$n_i(z, t) = \frac{\epsilon^2 Pe_i \lambda^2 p_l(z, t)}{16}, \quad i = m, c, e,$$

(C.15)

$$A_c(z, t) = c_l + B_m(z, t) \widehat{R}_m^{n_m} - B_c(z, t) \widehat{R}_m^{n_c} - \frac{m\mathcal{M} \widehat{R}_m^2}{2(n_c - 2)}$$

(C.16)

$$B_c(z, t) = -\frac{m\mathcal{M} \widehat{R}_c^{2-n_c}}{n_c(n_c - 2)},$$

(C.17)

$$B_m(z, t) = -\frac{\phi_c D_c}{\phi_m D_m} \frac{m\mathcal{M}}{n_m(n_c - 2)} (\widehat{R}_m^{n_c - n_m} \widehat{R}_c^{2-n_c} - \widehat{R}_m^{2-n_m}).$$

(C.18)

C.1. Numerical solution of the leading order system

The leading order system for the fluid flow, oxygen and lactate transport and cell layer growth is given by Eqs. (A.24)–(A.26) and (C.4)–(C.18). We solve this system numerically using the method of lines, i.e. by discretising the system in z (with a grid space of $\Delta z = 2 \times 10^{-3}$) and solving the resulting time-dependent ordinary differential equation (ODE) system using the MATLAB ODE solver `ode113`.

The algorithm for determining the cell layer growth can be summarised as follows:

1. Prescribe the initial position of the cell layer outer surface, i.e. set $\widehat{R}_c(z, 0) = \widehat{R}_{c,init}(z)$.
2. Determine the fluid pressures and velocities and solute concentrations throughout the bioreactor for the given position of the cell layer outer surface, by solving (C.4)–(C.6) for p_l (using the MATLAB boundary value problem solver `bvp4c`) and evaluating (C.7)–(C.18).
3. Evaluate the oxygen and lactate concentrations and shear stress at $r = \widehat{R}_c(z, t)$ and use these to update $\widehat{R}_c(z, t)$ according to the growth law (A.24).
4. Repeat Steps 1–3 until the simulation time (60 days) elapses, or the system reaches a steady state, or the cell layer grows to fill the entire ECS or recedes to the fibre surface (whichever occurs first).

The convergence of the numerical scheme was verified by reducing Δz and the time step and checking that the results were the same to a relative tolerance of 0.01%.

Appendix D. Reduced model for cell layer growth with ECS port closed

D.1. Fluid transport

When the ECS port is closed, the dimensionless boundary conditions on the ECS outer boundary are

$$u_{e,r} = 0, \quad u_{e,z} = 0 \text{ on } r = \widehat{R}_e.$$

(D.1)

Hence, at leading order in ϵ there is only flow in the lumen (steady Poiseuille flow) and no axial or radial flow in the rest of the bioreactor,

$$p_l(z, t) = 16(1 - z) + \widehat{P}_{l,out},$$

(D.2)

$$u_{l,z}(r, z, t) = 4(1 - r^2), \quad u_{l,r} = 0,$$

(D.3)

$$p_m(z, t) = \frac{p_l(z)}{\kappa_m}, \quad p_c(z, t) = \frac{p_l(z)}{\kappa_m \kappa_c},$$

(D.4)

$$u_{i,r}, u_{i,z} = 0, \quad i = m, c, e. \tag{D.5}$$

D.2. Mass transport

The reduced system for the solute transport with the ECS port closed (from (A.14) to (A.23)) is

$$4\epsilon^2 Pe_l(1 - r^2)\frac{\partial c_l}{\partial z} = \frac{1}{r}\frac{\partial}{\partial r}\left(r\frac{\partial c_l}{\partial r}\right), \tag{D.6}$$

$$0 = \frac{1}{r}\frac{\partial}{\partial r}\left(r\frac{\partial c_i}{\partial r}\right), \quad i = m, e, \tag{D.7}$$

$$0 = \frac{1}{r}\frac{\partial}{\partial r}\left(r\frac{\partial c_c}{\partial r}\right) + m\mathcal{M}, \tag{D.8}$$

where we have substituted for $u_{l,z}$ in (D.6) from (D.3) and used $u_{i,r}, u_{i,z} = O(\epsilon^2)$ ($i = m, c, e$) in (D.7) and (D.8). Integrating (D.7) and (D.8) and applying boundary conditions (A.19)–(A.20) yields

$$c_m(r, z, t) = \frac{\phi_c D_c}{\phi_m D_m}\frac{m\mathcal{M}}{2}(\widehat{R}_c(z, t)^2 - \widehat{R}_m^2)\ln r + C_m(z, t), \tag{D.9}$$

$$c_c(r, z, t) = \frac{m\mathcal{M}}{4}(2\widehat{R}_c(z, t)^2 \ln r - r^2) + C_c(z, t), \tag{D.10}$$

$$c_e(r, z, t) = \frac{m\mathcal{M}}{4}\widehat{R}_c(z, t)^2(2\ln\widehat{R}_c(z, t) - 1) + C_c(z, t), \tag{D.11}$$

where

$$C_c(z, t) = \frac{m\mathcal{M}}{4}\left(2\left(\frac{\phi_c D_c}{\phi_m D_m}(\widehat{R}_c(z, t)^2 - \widehat{R}_m^2) - \widehat{R}_c(z, t)^2\right)\times\ln\widehat{R}_m + \widehat{R}_m^2\right) + C_m(z, t), \tag{D.12}$$

and $C_m(z, t)$ is determined from the concentration continuity condition on the lumen–membrane interface in (A.18)

$$C_m(z, t) = c_l(1, z, t).$$

To close the system we need to solve the equation for the lumen concentration (D.6) subject to the boundary conditions (from (A.18) and (A.22))

$$\frac{\partial c_l}{\partial r}(0, z, t) = 0, \quad \frac{\partial c_l}{\partial r}(1, z, t) = \gamma(z, t), c_l(r, 0, t) = \begin{cases} 1 & \text{for oxygen} \\ 0 & \text{for lactate} \end{cases}, \quad \frac{\partial c_l}{\partial z}(r, 1, t) = 0, \tag{D.13}$$

where

$$\gamma(z, t) = \frac{\phi_c D_c}{D_l}\frac{m\mathcal{M}}{2}(\widehat{R}_c(z, t)^2 - \widehat{R}_m^2). \tag{D.14}$$

Since γ varies with z, we solve (D.6), (D.13)–(D.14) numerically.

D.3. Numerical solution of the leading order system

The leading order system for the fluid flow, oxygen and lactate transport and cell layer growth when the ECS port is closed is given by Eqs. (A.24)–(A.26), (D.3)–(D.5), (D.6) and (D.9)–(D.14). The algorithm used to solve this system is essentially the same as that used when the ECS port is open (Appendix C.1)—at each time step the steady flow and solute transport problems are solved for the current position of the outer surface of the cell layer, $r = \widehat{R}_c(z, t)$, and the solutions used to update $\widehat{R}_c$. However, in step 2 of the algorithm the advection–diffusion equation for the lumen concentration (D.6) is solved subject to (D.13)–(D.14), and (D.3)–(D.5) and (D.9)–(D.12) are used to determine the lumen pressure, lumen axial velocity and solute concentrations throughout the bioreactor. We solve (D.6) using the finite difference method with a grid of 501 by 201 nodes in the z- and r-directions respectively ($\Delta z = 2 \times 10^{-3}$, $\Delta r = 5 \times 10^{-3}$) and central difference approximations of the derivatives. The convergence of the numerical scheme was verified by reducing Δz and the time step and checking that the results were the same to a relative tolerance of 0.01%.

Appendix E. Flow profiles and solute distributions: uniform vs non-uniform cell layer

Figs. E1–E4 show the dimensional fluid pressure, flow velocity profiles and solute distributions for a rat cardiomyocyte layer with a uniform depth of 50 μm ($R_c(z, t) = 450$ μm) and one of the same volume whose depth decreases linearly from 80 μm to 19 μm along the fibre.
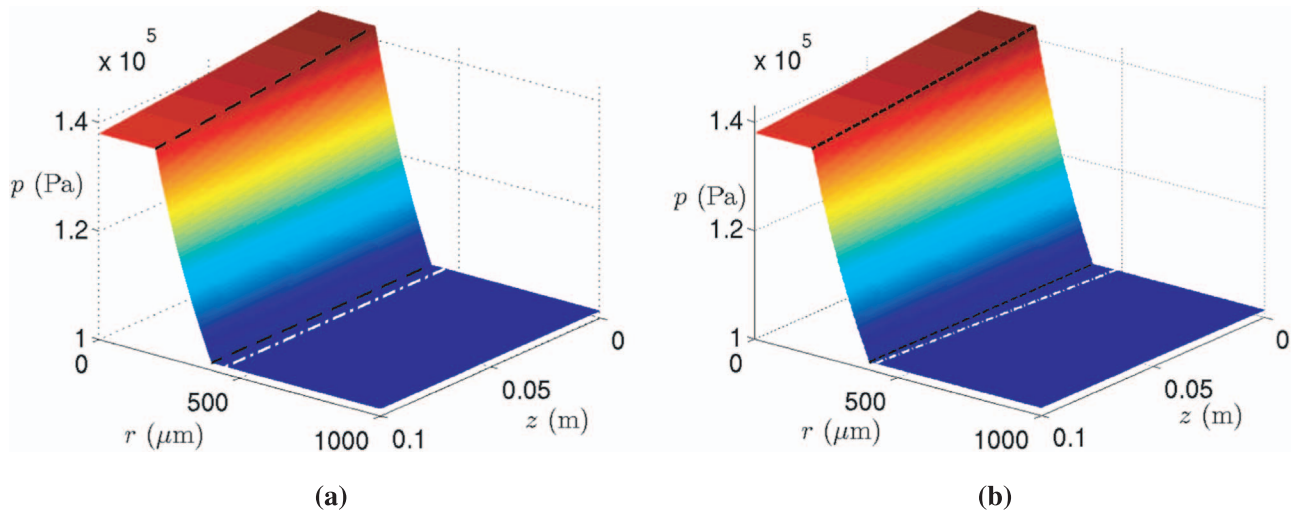
Fig. E1. Typical fluid pressure in the bioreactor, p, for (a) a uniform depth cell layer, $R_c = 450\,\mu m$ and (b) a non-uniform cell layer, $R_c = (480–6.1 \times 10^{-4}z)\,\mu m$. Parameter values: $Q_{l,in} = 3.33 \times 10^{-8}m^3\,s^{-1}$, $P_{l,out} = 1.379 \times 10^5$ Pa. All other parameter values as in Table 1. Lumen axis running from right to left. Black dashed lines indicate the membrane surfaces and the white dashed lines the outer surface of the cell layer.
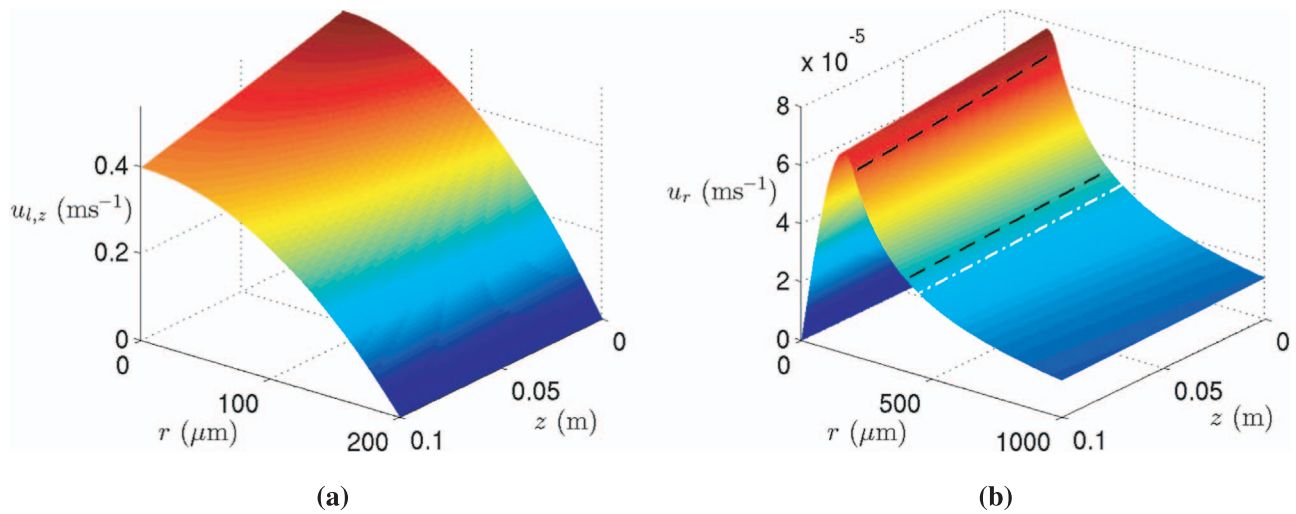

Fig. E2. (a) Lumen axial flow velocity $u_{l,z}$ and (b) radial flow velocity u_r for the uniform depth cell layer in Fig. E1(a). Profiles for the non-uniform cell layer in Fig. E1(b) are almost identical. All parameter values and dashed lines as in Fig. E1.
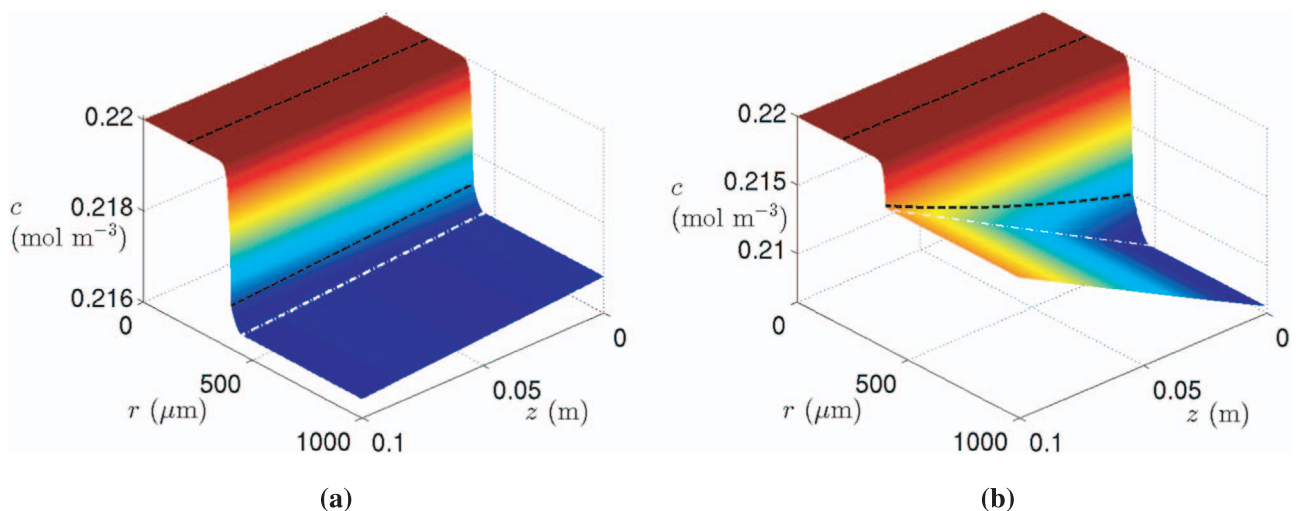

Fig. E3. Oxygen concentration in the bioreactor, c, for (a) the uniform depth rat cardiomyocyte layer and (b) the non-uniform depth rat cardiomyocyte layer. Fluid transport parameter values as in Fig. E1, and oxygen transport parameter values for rat cardiomyocytes as in Table 2. Dashed lines as in Fig. E1.
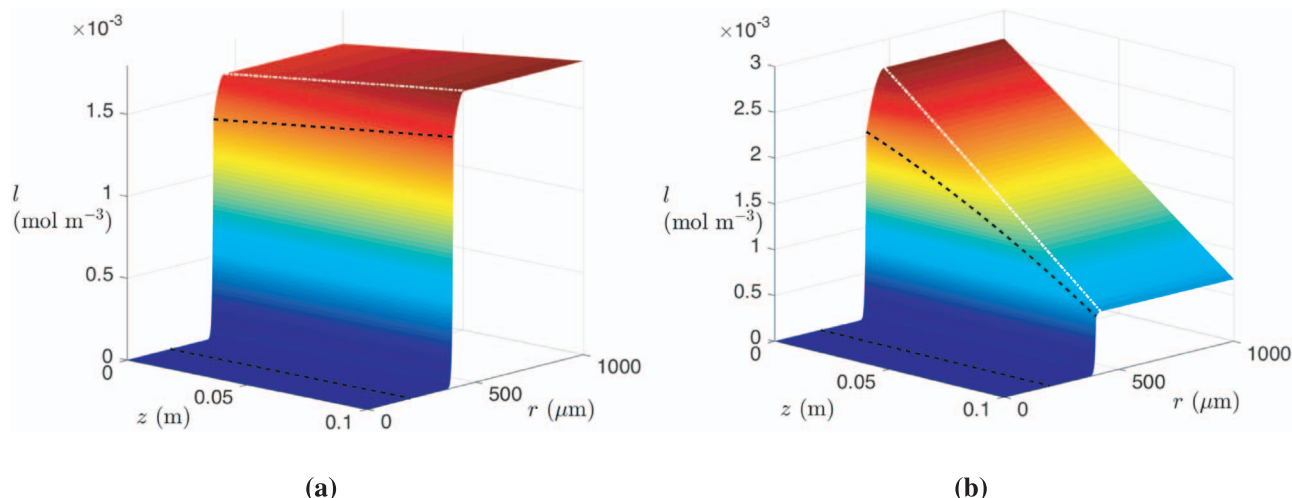
(a)   **(b)**

Fig. E4. Lactate concentration in the bioreactor, l, for (a) the uniform depth rat cardiomyocyte layer and (b) the non-uniform rat cardiomyocyte layer. Parameters as in Fig. E3 with $V_{max}^L = 1.32 \times 10^{-3}$ mol m^{-3}. Lumen axis running from left to right.

References

Abdullah, N.S., Das, D.B., 2007. Modelling nutrient transport in hollow fibre membrane bioreactor for growing bone tissue with consideration of multi-component interactions. Chem. Eng. Sci. 62 (21), 5821–5839.

Abdullah, N.S., Jones, D.R., Das, D.B., 2009. Nutrient transport in bioreactors for bone tissue growth: why do hollow fibre membrane bioreactors work? Chem. Eng. Sci. 64 (1), 109–125.

Azimi, B., Nourpanah, P., Rabiee, M., Arbab, S., 2014. Poly (lactide-co-glycolide) fiber: an overview. J. Eng. Fabr. Fibers 9 (1), 47–66.

Bear, J., 1988. Dynamics of Fluids in Porous Media. Dover Publications, New York.

Beavers, G., Joseph, D., 1967. Boundary conditions at a naturally permeable wall. J. Fluid Mech. 30 (1), 197–207.

Brotherton, J.D., Chau, P.C., 1996. Modeling of axial-flow hollow fiber cell culture bioreactors. Biotechnol. Prog. 12 (5), 575–590.

Carman, P.C., 1937. Fluid flow through granular beds. Trans. Inst. Chem. Eng. 15, 150–166.

Casciari, J.J., Sotirchos, S.V., Sutherland, R.M., 1992. Mathematical modelling of microenvironment and growth in EMT6/Ro multicellular tumour spheroids. Cell Prolif. 25 (1), 1–22.

Chapman, L.A.C., Shipley, R.J., Whiteley, J.P., Ellis, M.J., Byrne, H.M., Waters, S.L., 2014. Optimising cell aggregate expansion in a perfused hollow fibre bioreactor via mathematical modelling. PLoS ONE 9 (8), e105813.

Chen, G., Palmer, A., 2009. Hemoglobin-based oxygen carrier and convection enhanced oxygen transport in a hollow fiber bioreactor. Biotechnol. Bioeng. 102, 1603–1612.

Das, D.B., 2007. Multiscale simulation of nutrient transport in hollow fibre membrane bioreactor for growing bone tissue: sub-cellular scale and beyond. Chem. Eng. Sci. 62 (13), 3627–3639.

Davidson, A.J., Ellis, M.J., Chaudhuri, J.B., 2010. A theoretical method to improve and optimize the design of bioartificial livers. Biotechnol. Bioeng. 106 (6), 980–988.

De Napoli, I.E., Scaglione, S., Giannoni, P., Quarto, R., Catapano, G., 2011. Mesenchymal stem cell culture in convection-enhanced hollow fibre membrane bioreactors for bone tissue engineering. J. Membr. Sci. 379 (1), 341–352.

Eggleton, G.P., Eggleton, P., Hill, A.V., 1928. The coefficient of diffusion of lactic acid through muscle. Proc. R. Soc. Lond. B 103 (727), 620–628.

Elert, G., 2015. The Physics Hypertextbook. URL ⟨http://physics.info/⟩.

Ellis, M.J., Chaudhuri, J.B., 2007. Poly (lactic-co-glycolic acid) hollow fibre membranes for use as a tissue engineering scaffold. Biotechnol. Bioeng. 96 (1), 177–187.

Engel, F.B., Schebesta, M., Duong, M.T., Lu, G., Ren, S., Madwed, J.B., Jiang, H., Wang, Y., Keating, M.T., 2005. p38 MAP kinase inhibition enables proliferation of adult mammalian cardiomyocytes. Genes Dev. 19 (10), 1175–1187.

Fermor, B., Christensen, S.E., Youn, I., Cernanec, J.M., Davies, C.M., Weinberg, J.B., 2007. Oxygen, nitric oxide and articular cartilage. Eur. Cell Mater. 13, 56–65.

Galban, C.J., Locke, B.R., 1997. Analysis of cell growth in a polymer scaffold using a moving boundary approach. Biotechnol. Bioeng. 56 (4), 422–432.

Gray, W.G., 1975. A derivation of the equations for multi-phase transport. Chem. Eng. Sci. 30 (2), 229–233.

Guo, J., Jourdian, G.W., Maccallum, D.K., 1989. Culture and growth characteristics of chondrocytes encapsulated in alginate beads. Connect. Tissue Res. 19 (2–4), 277–297.

Hay, P.D., Veitch, A.R., Gaylor, J.D.S., 2001. Oxygen transfer in a convection-enhanced hollow fiber bioartificial liver. Artif. Organs 25 (2), 119–130.

Heath, C.A., Belfort, G., Hammer, B.E., Mirer, S.D., Pimbley, J.M., 1990. Magnetic resonance imaging and modeling of flow in hollow-fiber bioreactors. AIChE J. 36 (4), 547–558.

Holm, S., Maroudas, A., Urban, J.P.G., Selstam, G., Nachemson, A., 1981. Nutrition of the intervertebral disc: solute transport and metabolism. Connect. Tissue Res. 8 (2), 101–119.

Hoque, M.E., Chuan, Y.L., Pashby, I., 2012. Mathematical modelling on degradation of 3D tissue engineering scaffold materials. Regen. Res. 1 (1), 58–61.

Jones, A.F., Byrne, H.M., Gibson, J.S., Dold, J.W., 2000. A mathematical model of the stress induced during avascular tumour growth. J. Math. Biol. 40 (6), 473–499.

Kelsey, L., Pillarella, M., Zydney, A., 1990. Theoretical analysis of convective flow profiles in a hollow-fiber membrane bioreactor. Chem. Eng. Sci. 45 (11), 3211–3220.

Kim, B.-Y., Han, M.-J., Chung, A.-S., 2001. Effects of reactive oxygen species on proliferation of Chinese hamster lung fibroblast (V79) cells. Free Radic. Biol. Med. 30 (6), 686–698.

King, J., Franks, S., 2006. Mathematical modelling of nutrient-limited tissue growth. In: Free Boundary Problems. Springer, Basel, pp. 273–282.

Korin, N., Bransky, A., Dinnar, U., Levenberg, S., 2007. A parametric study of human fibroblasts culture in a microchannel bioreactor. Lab Chip 7 (5), 611–617.

Kozeny, J., 1927. Über kapillare leitung des wassers im boden. Sitzungsber. Akad. Wiss. Wien 136, 271–306.

Labecki, M., Bowen, B.D., Piret, J.M., 1996. Two-dimensional analysis of protein transport in the extracapillary space of hollow-fibre bioreactors. Chem. Eng. Sci. 51 (17), 4197–4213.

Labecki, M., Piret, J., Bowen, B., 2004. Effects of free convection on three-dimensional protein transport in hollow-fiber bioreactors. AIChE J. 50 (8), 1974–1990.

Leclerc, E., David, B., Griscom, L., Lepioufle, B., Fujii, T., Layrolle, P., Legallaisa, C., 2006. Study of osteoblastic cells in a microfluidic environment. Biomaterials 27 (4), 586–595.

Lee, D.A., Reisler, T., Bader, D.L., 2003. Expansion of chondrocytes for tissue engineering in alginate beads enhances chondrocytic phenotype compared to conventional monolayer techniques. Acta Orthop. 74 (1), 6–15.

Lewis, M.C., MacArthur, B.D., Malda, J., Pettet, G., Please, C.P., 2005. Heterogeneous proliferation within engineered cartilaginous tissue: the role of oxygen tension. Biotechnol. Bioeng. 91 (5), 607–615.

Lu, H., Lim, W.S., Zhang, P., Chia, S.M., Yu, H., Mao, H., Leong, K.W., 2005. Galactosylated poly (vinylidene difluoride) hollow fiber bioreactor for hepatocyte culture. Tissue Eng. 11 (11–12), 1667–1677.

Machide, M., Hashigasako, A., Matsumoto, K., Nakamura, T., 2006. Contact inhibition of hepatocyte growth regulated by functional association of the c-Met/hepatocyte growth factor receptor and LAR protein–tyrosine phosphatase. J. Biol. Chem. 281 (13), 8765–8772.

Malda, J., Rouwkema, J., Martens, D.E., Le Comte, E.P., Kooy, F.K., Tramper, J., Van Blitterswijk, C.A., Riesle, J., 2004. Oxygen gradients in tissue-engineered PEGT/PBT cartilaginous constructs: measurement and modeling. Biotechnol. Bioeng. 86 (1), 9–18.

McElwain, D.L.S., Ponzo, P.J., 1977. A model for the growth of a solid tumor with non-uniform oxygen consumption. Math. Biosci. 35 (3), 267–279.

Meneghello, G., 2010. Development of a Novel PVA-PLGA Hollow Fibre Bioreactor for Tissue Engineering (Ph.D. thesis). University of Bath.

Meneghello, G., Parker, D.J., Ainsworth, B.J., Perera, S.P., Chaudhuri, J.B., Ellis, M.J., De Bank, P.A., 2009. Fabrication and characterization of poly (lactic-co-glycolic acid)/polyvinyl alcohol blended hollow fibre membranes for tissue engineering applications. J. Membr. Sci. 344 (1–2), 55–61.

Murrell, G.A., Francis, M., Bromley, L., 1990. Modulation of fibroblast proliferation by oxygen free radicals. Biochem. J. 265, 659–665.

Nyberg, S.L., Remmel, R.P., Mann, H.J., Peshwa, M.V., Hu, W.S., Cerra, F.B., 1994. Primary hepatocytes outperform Hep G2 cells as the source of biotransformation functions in a bioartificial liver. Ann. Surg. 220 (1), 59–67.

Obradovic, B., Carrier, R.L., Vunjak-Novakovic, G., Freed, L.E., 1999. Gas exchange is essential for bioreactor cultivation of tissue engineered cartilage. Biotechnol. Bioeng.

63 (2), 197–205.

Patzer, J.F., II, 2004. Oxygen consumption in a hollow fiber bioartificial liver-revisited. Artif. Organs 28 (1), 83–98.

Pearson, N.C., Oliver, J.M., Shipley, R.J., Waters, S.L., 2015a. A multiphase model for chemically- and mechanically-induced cell differentiation in a hollow fibre membrane bioreactor: minimising growth factor consumption. Biomech. Model. Mechanobiol., 1–18.

Pearson, N.C., Shipley, R.J., Waters, S.L., Oliver, J.M., 2014. Multiphase modelling of the influence of fluid flow and chemical concentration on tissue growth in a hollow fibre membrane bioreactor. Math. Med. Biol. 31 (4), 393–430.

Pearson, N.C., Waters, S.L., Oliver, J.M., Shipley, R.J., 2015b. Multiphase modelling of the effect of fluid shear stress on cell yield and distribution in a hollow fibre membrane bioreactor. Biomech. Model. Mechanobiol. 14 (2), 387–402.

Pillarella, M.R., Zydney, A.L., 1990. Theoretical analysis of the effect of convective flow on solute transport and insulin release in a hollow fiber bioartificial pancreas. J. Biomech. Eng. 112, 220–228.

Piret, J.M., Cooney, C.L., 1991. Model of oxygen transport limitations in hollow fiber bioreactors. Biotechnol. Bioeng. 37 (1), 80–92.

Quintard, M., Whitaker, S., 1994. Convection, dispersion, and interfacial transport of contaminants: homogeneous porous media. Adv. Water Resour. 17 (4), 221–239.

Radisic, M., Deen, W., Langer, R., Vunjak-Novakovic, G., 2005. Mathematical model of oxygen distribution in engineered cardiac tissue with parallel channel array perfused with culture medium containing oxygen carriers. Am. J. Physiol. – Heart Circ. Physiol. 288 (3), H1278–H1289.

Sankar, K.S., Green, B.J., Crocker, A.R., Verity, J.E., Altamentova, S.M., Rocheleau, J.V., 2011. Culturing pancreatic islets in microfluidic flow enhances morphology of the associated endothelial cells. PLoS ONE 6 (9), e24904.

Schonberg, J.A., Belfort, G., 1987. Enhanced nutrient transport in hollow fiber perfusion bioreactors: a theoretical analysis. Biotechnol. Prog. 3 (2), 80–89.

Shipley, R.J., Davidson, A.J., Chan, K., Chaudhuri, J.B., Waters, S.L., Ellis, M.J., 2011. A strategy to determine operating parameters in tissue engineering hollow fiber bioreactors. Biotechnol. Bioeng. 108 (6), 1450–1461.

Shipley, R.J., Ellis, M.J., Waters, S.L., 2009. Combining mathematical modelling with experimental data to characterize fluid and protein transport properties in hollow fibre scaffolds. In: Proceedings of ITP-09 (Interdisciplinary Transport Phenomena VI).

Shipley, R.J., Waters, S.L., 2012. Fluid and mass transport modelling to drive the design of cell-packed hollow fibre bioreactors for tissue engineering applications. Math. Med. Biol. 29 (4), 329–359.

Shipley, R.J., Waters, S.L., Ellis, M.J., 2010. Definition and validation of operating equations for poly (vinyl alcohol)-poly (lactide-co-glycolide) microfiltration membrane-scaffold bioreactors. Biotechnol. Bioeng. 107 (2), 382–392.

Smith, R.L., Donlon, B., Gupta, M., Mohtai, M., Das, P., Carter, D., Cooke, J., Gibbons, G., Hutchinson, N., Schurman, D., 1995. Effects of fluid-induced shear on articular chondrocyte morphology and metabolism in vitro. J. Orthop. Res. 13 (6), 824–831.

Stabler, C.L., Fraker, C., Pedraza, E., Constantinidis, I., Sambanis, A., 2009. Modeling and in vitro and in vivo characterization of a tissue engineered pancreatic substitute. J. Comb. Optim. 17 (1), 54–73.

Sullivan, J.P., Gordon, J.E., Bou-Akl, T., Matthew, H.W.T., Palmer, A.F., 2007. Enhanced oxygen delivery to primary hepatocytes within a hollow fiber bioreactor facilitated via hemoglobin-based oxygen carriers. Artif. Cells Blood Substit. Biotechnol. 35 (6), 585–606.

Sullivan, J.P., Gordon, J.E., Palmer, A.F., 2006. Simulation of oxygen carrier mediated oxygen transport to C3A hepatoma cells housed within a hollow fiber bioreactor. Biotechnol. Bioeng. 93 (2), 306–317.

Takamiya, M., Haider, K.H., Ashraf, M., 2011. Identification and characterization of a novel multipotent sub-population of Sca-1+ cardiac progenitor cells for myocardial regeneration. PLoS ONE 6 (9), e25265.

Tharakan, J.P., Chau, P.C., 1986. A radial flow hollow fiber bioreactor for the large-scale culture of mammalian cells. Biotechnol. Bioeng. 28 (3), 329–342.

Tomita, M., Sato, E.F., Nishikawa, M., Yamano, Y., Inoue, M., 2001. Nitric oxide regulates mitochondrial respiration and functions of articular chondrocytes. Arthritis Rheum. 44 (1), 96–104.

Tziampazis, E., Sambanis, A., 1995. Tissue engineering of a bioartificial pancreas: modeling the cell environment and device function. Biotechnol. Prog. 11 (2), 115–126.

Wang, D.W., Fermor, B., Gimble, J.M., Awad, H.A., Guilak, F., 2005. Influence of oxygen on the proliferation and metabolism of adipose derived adult stem cells. J. Cell. Physiol. 204 (1), 184–191.

Whittaker, R.J., Booth, R., Dyson, R., Bailey, C., Parsons Chini, L., Naire, S., Payvandi, S., Rong, Z., Woollard, H., Cummings, L.J., Waters, S.L., Mawasse, L., Chaudhuri, J.B., Ellis, M.J., Michael, V., Kuiperk, N.J., Cartmell, S., 2009. Mathematical modelling of fibre-enhanced perfusion inside a tissue-engineering bioreactor. J. Theor. Biol. 256 (4), 533–546.

Wung, N., Acott, S.M., Tosh, D., Ellis, M.J., 2014. Hollow fibre membrane bioreactors for tissue engineering applications. Biotechnol. Lett. 36 (12), 2357–2366.

Ye, H., Das, D.B., Triffitt, J.T., Cui, Z., 2006. Modelling nutrient transport in hollow fibre membrane bioreactors for growing three-dimensional bone tissue. J. Membr. Sci. 272 (1–2), 169–178.

Ye, H., Xia, Z., Ferguson, D.J.P., Triffitt, J.T., Cui, Z., 2007. Studies on the use of hollow fibre membrane bioreactors for tissue generation by using rat bone marrow fibroblastic cells and a composite scaffold. J. Mater. Sci.: Mater. Med. 18 (4), 641–648.